NASA TECHNICAL MEMORANDUM

NASA TM X-52570

NASA TM X-52570

PERFORMANCE OF A 10° CONICAL PLUG NOZZLE USING A TURBOJET GAS GENERATOR

by Sidney C. Huntley and Nick E. Samanich
Lewis Research Center
Cleveland, Ohio

March 1969

This information is being published in preliminary form in order to expedite its early release.

ABSTRACT

Internal performance data were obtained over a pressure ratio range from 2 to 30 and corrected secondary weight flow ratios from 2 to 8% with shrouds up to about 1/4 the total plug length and with plug truncations of 100%, 75%, and 50% of full length plug. The results indicate thrust coefficients of 98% and 97.5% were possible at low and high pressure ratios, respectively. Half of a 2% thrust loss with 50% plug was regained by removal of base and venting cavity. Individual thrust components are shown.

PERFORMANCE OF A 10° CONICAL PLUG NOZZLE

USING A TURBOJET GAS GENERATOR

by Sidney C. Huntley and Nick E. Samanich

Lewis Research Center
Cleveland, Ohio

SUMMARY

A 10° conical plug nozzle installed on a J85-GE-13 turbojet engine was tested in an altitude facility at the NASA-Lewis Research Center. Cylindrical outer shrouds were used to adjust the internal expansion of the nozzle up to an internal expansion pressure ratio of 22.

The isentropic thrust coefficient was found to be about 98 percent with moderate amounts of secondary air flow at low pressure ratios (≈ 3) and about 97.5 percent at high pressure ratios (> 20). A 1/2 percent loss in thrust was encountered at low pressure ratios when the plug was truncated to 3/4 of the original length. Truncating the plug to 1/2 of its original length resulted in a performance loss of 2% at low pressure ratio. Removal of the base on the 50% plug and venting the cavity with a percent or two of secondary air resulted in a 1% gain in performance. Truncating the plug with the longer shrouds did not have an adverse effect on thrust at high pressure ratios. Pumping characteristics were limited by a choking condition in the secondary exit with short shrouds or by primary flow attachment in the long shrouds.

A breakdown of the individual thrust components showed the plug (and base of truncated plugs) contributed from 1 to 3 points toward thrust coefficient with short shrouds. Addition of the long shroud doubled the plug contribution and provided a similar increase in thrust from the increased pressure level on the primary nozzle boattail.

INTRODUCTION

The Lewis Research Center has initiated a flight research program to determine propulsion system installation effects for a broad spectrum of airbreathing engine nozzles applicable to supersonic cruise flight. The program consists of flight testing nozzles in the subsonic, transonic and low supersonic speed ranges, using an F-106 aircraft with two 25-inch (63.50 cm) diameter underwing nacelles containing J85 turbojet engines. Installation effects on thrust and drag of a research nozzle in one nacelle can be determined by comparing performance data obtained during flight with a reference nozzle in the other nacelle. In order to achieve this comparison, the internal performance of each nozzle must first be defined. This report documents the internal performance of a 10° conical plug nozzle with several external cylindrical shrouds as run in the Propulsion System Laboratory (PSL) altitude chamber of the Lewis Research Center. The performance was obtained with the nozzle attached to a simulated flight test nacelle assembly (including a J85 turbojet engine).

internal thrust and pumping characteristics, some typical pressure and temperature profiles along the plug, and some thrust component forces were obtained. Variations of secondary cooling air flow rates were made to determine the effect on performance. Plug truncations of 3/4 and 1/2 of the original length were also tested. In one instance, the base cap was removed from the 50% plug to determine the effect on performance of venting the plug cavity with a small percentage of secondary air. The J85 turbojet engine was operated at rated engine speed with no afterburning to provide primary gas flow to the plug nozzle. A separate metered supply was used for secondary air flow. Maximum nozzle pressure ratios of 30 were obtained.

APPARATUS AND PROCEDURE

Installation

A schematic view and photograph of the research hardware installation in the Propulsion Systems Laboratory altitude chamber are shown in figures 1 and 2. A view of the full-length plug extending into the exhaust duct is shown in figure 3. A J85-GE-13 turbojet engine with afterburner, modified by removing its variable area nozzle, and used as a gas generator for the plug nozzle was mounted within a nacelle. The plug nozzle was attached to the afterburner outlet using a packing gland slip joint. The nacelle which also supported the plug nozzle and shroud assembly was mounted from a bed plate freely suspended by four flexure rods. Pressure forces acting on the engine, nozzle, and nacelle were transmitted to a load cell used to measure thrust. The load cell was water cooled to provide a constant temperature environment and eliminate errors in the cell due to heating of the test section during engine operation. A minimal amount of air was admitted to the test section of the altitude chamber through a bypass valve to reduce heating and keep the test section at an acceptable temperature level. A front bulkhead with a labyrinth seal around the inlet section of the primary air venturi separated the engine inlet air from the exhaust and provided a means of adjusting exhaust pressure independent of inlet pressure. A flow deflector (not shown) was used to divert air leakage through the seal from impinging on the nacelle. Pressure measurements on either side of the labyrinth seal were used to obtain the seal force applied to the thrust load cell.

Measured amounts of secondary nozzle air flow were supplied to a toroidal manifold and entered the front of the nacelle to cool the engine and primary nozzle. A rotary valve at the front of the nacelle was used to regulate upstream secondary air pressure to the same value as engine inlet air pressure.

Plug Nozzle

A photograph of the plug expanded to its separate components is shown in figure 4. Plug nozzle dimensions are shown in figure 5. The

10^o half-angle plug was tested with a 17^o half-angle primary conical nozzle which simulated an iris-type nozzle with a flow area of 110 in.^{2} (710 cm^2). Both the plug and primary nozzle were attached to the 25 in. (63.50 cm) diameter nacelle. Simulation of a translating shroud was achieved using five different extensions to the nacelle (figure 6). Sections of the plug were removable and base caps were provided to truncate the plug at 75% and 50% of its full length. For one test configuration the base cap for the 50% plug truncation was removed.

The plug and primary nozzle attachment to the nacelle was accomplished using three equally spaced hollow struts (located at $\phi = 0^o$, 120^o and 240^o) which also provided passageways for instrumentation leads. (Symbols used in this report are defined in Appendix A). The passageways also provided a means of pressurizing the plug cavity with secondary air. With the 50% plug base cap removed, approximately one to two percent of the secondary air was estimated to flow into the cavity.

Instrumentation

Static pressures in the primary air venturi (station 1) and total pressure and temperature ahead of the bellmouth were used to obtain inlet momentum and engine air flow. Metered engine fuel flow was added to engine air flow to obtain the primary nozzle gas flow. Primary nozzle gas temperature was assumed equal to the measured turbine discharge temperature (station 5). Primary nozzle gas total pressure (station 8) was assumed to be 94.8% of the measured turbine discharge total pressure. This pressure loss was based on an engine calibration with a jet nozzle area of 110 in^2 (710 cm^2). (reference 1).

Two standard ASME sharp-edged orifices were used to determine the secondary nozzle air flow. Secondary nozzle total pressure was measured about one nacelle diameter ahead of the secondary air exit (figure 6a).

Static pressure taps and thermocouples were installed at the secondary exit, primary nozzle boattail and along the plug (figure 6). The longest shroud ($x/L = 0.229$) had internal static pressure taps and thermocouples. Each base cap used to truncate the plug was equipped with static pressure taps and thermocouples. When the 50% plug base cap was removed, an internal pressure probe was used to obtain the cavity pressure.

Procedure

Engine inlet pressure was maintained at static sea level for all data except for that with the second shortest shroud ($x/L = -.080$) in which case inlet pressure corresponded to a flight Mach number of 0.9 at an altitude of 25,000 ft. (7620 m). Engine inlet air and secondary

air were supplied at a nominal temperature of 535°R (297°K). The engine was operated at rated speed (16,500 rpm) for all data, and (with no afterburning) provided a primary nozzle gas flow of 44 lbs/sec (19.96 kg/sec) at a temperature of 1660°R (922°K).

Performance characteristics of each nozzle configuration, consisting of a particular plug truncation and shroud combination, were investigated over a range of nozzle pressure ratios deemed appropriate for the particular shroud length.

The short shrouds (x/L = -.120, -.080, .008) were tested over a range of nozzle pressure ratios from 2 to 22; the long shrouds (x/L = .132 and .229) up to 30. Nozzle pressure ratio was varied by changing the altitude pressure. At each setting of nozzle pressure ratio, the secondary air flow was adjusted to each of three values covering a nominal range of 2 to 8 percent corrected secondary weight flow ratio, $\omega\sqrt{\tau}$. At each setting of secondary air flow, the secondary air pressure upstream of the rotary valve at the nacelle inlet was adjusted to the same value as engine inlet air pressure.

Methods used for data reduction are discussed in Appendix B.

RESULTS AND DISCUSSION

Thrust coefficients, secondary total pressure ratios, and nozzle pressure ratios for each nozzle configuration were plotted as a function of corrected secondary weight flow ratio, $\omega\sqrt{\tau}$. Values of each of these parameters were then interpolated or extrapolated to obtain values at corrected secondary weight flow ratios of .02, .04, .06, and .08. These values are represented in figures 7 through 12 by symbols for each shroud length. The symbols on these curves are therefore not necessarily actual data points. Actual data points were selected for figures 13 through 19.

Thrust Characteristics

Thrust characteristics of the plug nozzle are presented in figure 7 through 9 as a function of nozzle pressure ratio for corrected secondary weight flow ratios of .02, .04, .06, and .08. Thrust characteristics are presented for each of several shroud lengths and for each plug truncation, 100%, 75%, and 50%. Thrust coefficients are shown in two forms, isentropic thrust coefficient, Fg/(Fip + Fis), and primary thrust coefficient, Fg/Fip, where Fg is actual jet thrust, Fip is the ideal thrust of the primary flow, and Fis is the ideal thrust of the secondary flow. Fis was set to zero when the secondary total pressure was less than altitude pressure. The discussion of thrust in this report will only refer to the isentropic thrust coefficient, Fg/Fip + Fis).

In general, thrust characteristics for each corrected secondary weight flow ratio and for each plug truncation exhibited similar trends.

With the 100% plug, isentropic thrust coefficient was about 98 percent at a nozzle pressure ratio of 3 and decreased with increasing nozzle pressure ratios with the short shrouds (x/L = .008 or less) indicating the nozzle flow was undergoing free expansion. As nozzle pressure increased the primary expansion remained attached to the plug for a greater distance downstream resulting in some benefit to thrust above that from free expansion alone. Secondary flow had no significant effect on jet thrust in these cases because it was free to expand outward.

Truncating the plug to 75% of its full length decreased the thrust level with the short shrouds about 1/2% (figs. 7 and 8). Truncating the plug to 50% (figure 9), however, resulted in a 2% loss in thrust coefficient at the low levels of nozzle pressure ratio. Removing the base cap of the 50% plug increased the thrust coefficient about 1% above that with the base cap. The plug cavity was connected to the secondary flow channel by 3 hollow supporting struts which were also used for instrumentation leads. A flow area of about 2.7 in^2 (17.42 cm^2) was available in these struts to vent the cavity with secondary air. This flow area represents about 2% of the annulus area available for secondary air flow and consequently only a percent or 2 of the secondary air was estimated to vent the cavity.

The addition of a long shroud (x/L = .132 or .229) resulted in internal expansion of the primary flow at high nozzle pressure ratios. The one-dimensional "design pressure ratio" was increased to 18 (with x/L = .132) and to 22 (with x/L = .229) which also increased the isentropic thrust coefficient at corresponding nozzle pressure ratios. Secondary flow had a significant effect on jet thrust resulting in an increase in thrust with increase in flow from 2 to about 6%. The thrust performance peaked at about .975 with corrected secondary weight flow ratios of about .06.

Truncating the plug with the longer shrouds did not have an adverse effect on thrust.

Pumping Characteristics

The pumping characteristics are presented in figures 10, 11, and 12 for corrected secondary weight flow ratios of .02, .04, .06, and .08; for each of several shroud lengths; and, for plug truncations of 100%, 75%, and 50%. In general, secondary total pressure ratio decreased to a limiting value as nozzle pressure ratio was increased. The limiting value of secondary total pressure ratio was dependent on shroud length and corrected secondary weight flow ratio. Truncation of the plug had no effect on pumping characteristics. The effect of shroud length on pumping decreased with increasing corrected secondary weight flow ratio. The lowest secondary total pressure ratio was attained with the short shrouds (x/L = .008 and less) at low secondary weight flow. Attainment

of a limiting condition of pumping pressure with a short shroud indicates the secondary exit became choked. The limiting condition of pumping with the long shrouds (x/L = .132 and .229) occurred at higher levels of secondary total pressure ratio. This occurrence indicates the expansion of the primary flow had effectively attached to the shroud and a decrease in altitude pressure was no longer sensed upstream of the point of attachment. Data were not obtained with the longest shroud (x/L = .229) where the primary flow was not "attached" to the shroud.

Typical pressure and temperature distributions with the longest shroud (x/L = .229) are presented in figure 13. Axial static pressure distributions are shown both along the shroud and along the primary nozzle boattail. Also shown are the secondary total pressure (measured at x/L = -.634), the altitude pressure and the axial shroud temperature distributions. Data are presented for three secondary air flows at the lowest nozzle pressure ratio tested (figure 13a) and at the next lowest (figure 13b). At a nozzle pressure ratio of 5.4 (figure 13a), the shroud static pressure increased for a short distance, then decreased and near the end of the shroud increased again to approach the altitude pressure. The shroud static pressure increased with increasing secondary flow indicating less expansion of the primary stream, whereas the difference between secondary total and wall static pressures indicate the secondary stream was accelerated. Primary nozzle boattail static pressures agreed with the shroud statics. An increase in nozzle pressure ratio to 11.0 (fig. 13b) did not change the pressure distributions in the upstream half of the shroud but significantly affected the flow near the shroud exit (station 9) because altitude pressure was relatively lower. Further increases in nozzle pressure ratio did not alter the pressure distribution along the shroud. Shroud temperatures increased with increasing distance from the nozzle throat but the general level of temperatures decreased with increasing secondary flow.

Pressure and Temperature Distributions on Plug

Some typical pressure and temperature distributions on the plug are presented in figures 14 and 15 for several nozzle pressure ratios and plug truncations. Also presented are the corresponding altitude pressures and average base pressure and temperature for the truncated plugs. The expansion of static pressure on the plug from critical nozzle pressure to altitude pressure occurred within a relatively short distance downstream of the nozzle throat. At a nozzle pressure ratio of 2.1, plug pressure remained relatively constant with a slight over-expansion near the nozzle throat and a gradual increase to altitude pressure. As nozzle pressure ratio increased to 3.8 (or altitude pressure decreased) overexpansions and recompressions resulted in large pressure fluctuations along the plug. With a further increase in nozzle pressure ratio the overexpansions and recompressions appeared to move downstream on the plug and diminish in magnitude and frequency. Temperatures along the plug length remained near primary nozzle temperature with some evidence of reducing only at nozzle pressure ratios greater than 5. At the high values of nozzle pressure ratio the skin temperature appeared to

reflect the static temperature of the primary flow. That is, a rise in static pressure indicative of a reduction in primary gas velocity resulted in an increase in plug temperature. The pressure and temperature distributions along the plug were not affected by plug truncation. Furthermore, base pressure and temperature appeared to reflect plug pressure at the point of truncation. With the long shroud and a high nozzle pressure ratio (25 or greater) the expansion within the length of the shroud (x/L = .229) appeared to follow a smooth expansion with recompression occurring at the shroud exit.

Pressure surveys along the plug were made at several angular locations. Some typical differences in circumferential pressure are shown in figure 15. The deviation in circumferential pressure appeared to result primarily from strut wakes.

Thrust Components

The contribution to jet thrust from both primary and secondary gas flow, calculated by the method discussed in Appendix B -- Data Reduction, is presented in figure 16. The sum of primary and secondary thrust divided by the isentropic thrust of both primary and secondary flows is shown as a function of nozzle pressure ratio for data obtained with the full-length plug, a moderate amount of secondary airflow and with the several shroud lengths. The primary and secondary thrust contribution to jet thrust displays the typical decrease in thrust with increasing nozzle pressure ratio resulting from losses associated with free expansion. As expected, shroud length had no effect on the primary and secondary thrust referenced to altitude pressure. Although not shown, the primary and secondary thrust was also independent of plug truncation. The low value of calculated thrust at a nozzle pressure ratio of 2 resulted from the primary thrust calculation and occurred with all plug truncations at low nozzle pressure ratios. This problem was attributed to a change in primary nozzle characteristics at near sonic flow not accounted for in the calculations.

The calculated jet thrust contribution from the plug and base of truncated plugs is presented in figure 17 as a function of nozzle pressure ratio. The individual contribution of base thrust is also shown for the truncated plugs. The sum of plug and base thrust increased rapidly at low pressure ratios up to a pressure ratio of about 6 after which the plug forces increased at a constant lower rate. Because the plug contribution was considered to start from the "throat" of the primary nozzle, the values of plug thrust at low pressure ratio are also subject to change in primary nozzle characteristics at near sonic flows. With the short shrouds (x/L = .008 and less) the plug contributed from about 1 to 3 points toward the isentropic thrust coefficient during operation above nozzle pressure ratios of about 6. Extending the shroud behind the primary exit (x/L = .132 and .229) resulted in contributions up to double that of the short shrouds. This increase in thrust is attributed to more complete expansion along the plug with added guidance of flow through the shrouds. Base thrust was negligible with the 75% plug and generally created a drag force of about 1/2 point with the 50% plug

truncation.

The primary nozzle boattail thrust is presented in figure 18 for the several shrouds with the 100% plug. With the two shortest shrouds (x/L = -.120 and -.080) the boattail remained at altitude pressure over the range of nozzle pressure ratios tested and consequently there was no force or drag contribution to jet thrust. Extending the shroud to the primary exit plane (x/L = .008) created a drag on the boattail of about a 1/2 point. While not calculated, it is anticipated this drag would vary as a function of secondary flow. The data presented are for a nominal amount of secondary flow and consequently represents near optimum jet thrust conditions. Further extensions of the shroud (x/L = .132 and .229) resulted in a major addition to the jet thrust similar to that from the plug at high nozzle pressure ratios. As previously shown for the longest shroud (figure 13), boattail static pressures remained essentially constant with increasing nozzle pressure ratio over the range tested. The increase in boattail thrust with increasing nozzle pressure ratio consequently reflects the reduction in altitude pressure.

The total of the individual calculated contributions to jet thrust are compared with the actual jet thrust calculated from load cell measurements in figure 19. The ratio of calculated to actual jet thrust is presented as a function of nozzle pressure ratio for the several shrouds and plug truncations. The calculated thrust is generally within 1/2 percent of actual thrust for all cases above nozzle pressure ratios of 4. As nozzle pressure ratio decreased below 4, the accuracy of calculated thrust decreased rapidly. This rapid decrease in thrust is attributed to a change in primary nozzle characteristics at near sonic velocities not accounted for in the calculation methods used in this report.

CONCLUDING REMARKS

1. An isentropic thrust coefficient of 98 percent was achieved with moderate amounts of secondary weight flow at low pressure ratios ($\approx$ 3) using a short cylindrical shroud (x/L = .008). The addition of a longer shroud (x/L = .229) resulted in a thrust coefficient of 97.5 percent at high pressure ratios ($>$ 20).

2. A 1/2 percent loss in thrust coefficient was encountered at low pressure ratio when the plug was truncated to 3/4 of the original length. Truncating the plug to 1/2 of its original length resulted in a 2% loss in thrust coefficient with short shrouds at low pressure ratio. Removing the base cap of the 50% plug and venting with (possibly a percent or two) secondary air resulted in a 1% gain in thrust coefficient with a short shroud at low pressure ratio. Truncating the plug with the longer shrouds did not have an adverse effect on thrust at high pressure ratios.

3. Pumping characteristics of the plug nozzle were limited by a choking condition in the secondary exit with short shrouds or by primary flow attachment in the long shrouds. Truncating the plug had no effect on pumping characteristics.

4. A breakdown of the individual thrust components showed the plug (and base of truncated plugs) contributed from 1 to 3 points towards thrust coefficient with short shrouds. Addition of the long shroud doubled the plug contribution and provided a similar increase in thrust from the increased pressure level on the primary nozzle boattail.

APPENDIX A

Symbols

d - nacelle diameter

D - diameter

Fg - actual jet thrust

Fip - isentropic primary thrust

Fis - isentropic secondary thrust

°K - Kelvin (temperature)

L - length of full-length plug from nozzle throat

Pbt - primary nozzle boattail static pressure

po - simulated altitude static pressure

pp - plug static pressure

psh - shroud static pressure

Pt8 - primary nozzle total pressure

Pts - secondary total pressure

°R - Rankine (temperature)

R - radius

T8 - primary nozzle total temperature

Tp - plug skin temperature

Tsh - shroud skin temperature

x - distance downstream from nozzle throat

τ - total temperature ratio of secondary air to primary gas

ϕ - angular location clockwise from top looking upstream

ω - weight flow ratio of secondary air to primary gas

APPENDIX B - DATA REDUCTION

Experimental Data

The primary nozzle gas flow was obtained using calibrated fuel flow meters and a calibrated air venturi.

Secondary air total temperature at the secondary exit (figure 6) was calculated from continuity using the measured mass flow, total pressure, static pressure, and flow area. A constant ratio of specific heats of 1.4 was assumed.

Actual jet thrust, F_g, was calculated from the load cell measurements corrected for tare forces (reference 1). Tare forces consisting of inlet air momentum and pressure forces were obtained from prior calibrations of the installation. The ideal jet thrust of each stream was calculated from the measured mass flow rate expanded isentropically from the measured total pressure to altitude pressure (reference 2). The ideal secondary jet thrust was set to zero if the secondary total pressure was less than altitude pressure. Review of the data showed that this occurred at only a few points at low secondary air flow rates and at low nozzle pressure ratios. An isentropic thrust coefficient was obtained as the ratio of the actual jet thrust to the sum of the ideal jet thrust of both primary and secondary flows. A primary thrust coefficient was also obtained as the ratio of actual jet thrust to the ideal jet thrust of the primary gas flow.

The thrust coefficients, secondary total pressure ratio, and the nozzle pressure ratio for each nozzle configuration were plotted as a function of corrected secondary weight flow ratio $\omega\sqrt{\tau}$. Values of each of these parameters were then interpolated or extrapolated to obtain parameters at corrected secondary weight flow ratios of 0.02, .04, .06, and .08. These values are represented in figures 7 through 12 by symbols for each shroud length. The symbols on these curves are therefore not necessarily actual data points. Actual data points were selected for figures 13 through 19.

Computed Thrust Components

Individual contributions to jet thrust were calculated for some typical actual data. Nozzle dimensions (fig. 5) obtained at room temperature were corrected for thermal expansion by using a nominal temperature of 1660°R (922°K) for the plug and primary nozzle and a nominal temperature of 730°R (406°K) for the shrouds. Because the plug and primary nozzle were both attached to the three struts, the axial thermal growth of both were assumed to be the same. Boattail drag resulting from the

thin shrouds (about 1% of the total nacelle area) was insignificant for these static tests. The remaining nacelle area was appropriately divided between secondary exit flow area, primary nozzle boattail area, axial component of primary exit flow area, plug area and plug base area. Location of the position of the primary throat on the plug was determined from interpolation of plug pressure as a function of axial location (see figure 14). Axial location of pressure taps were determined at room temperature but under actual test conditions critical pressure ratio on the plug occurred slightly downstream of the "room temperature" throat. An axial location of $x/L = 0.01$ was established as the position of the primary throat during tests.

The contribution to jet thrust from primary gas flow was calculated assuming critical flow and using the gas properties, measured mass flow and measured temperature to obtain the total momentum at the nozzle throat. The stream was assumed to follow the 10° half-angle plug and a correction was applied to the total momentum to obtain the axial component. The primary thrust contribution was then obtained by subtracting the product of altitude pressure and primary exit flow area (normal to axis).

The contribution to jet thrust from secondary air flow was calculated using a constant ratio of specific heats of 1.4, measured secondary exit static pressure, measured secondary total pressure, and the secondary exit flow area. The secondary thrust contribution was then obtained by subtracting the product of altitude pressure and secondary exit flow area.

The thrust contribution of the plug and base of truncated plugs were calculated by the difference between plug pressures (or base pressures) and altitude pressure integrated over the appropriate area. Thrust contribution of the primary nozzle boattail was obtained in a similar manner.

Each of the calculated contributions were normalized to the sum of isentropic thrust of both the primary and secondary flows. The sum of the calculated thrust was also divided by the actual jet thrust for comparative purposes.

REFERENCES

1. Antl, Robert J. and Burley, Richard R.: Steady-State Airflow and Afterburning Performance Characteristics of Four J85-GE-13 Turbojet Engines. NASA TM X-1742, 1969.

2. Trout, Arthur M.; Papell, S. Stephen; and Povolny, John H.: Internal Performance of Several Divergent-Shroud Ejector Nozzles with High Divergence Angles. NACA RM E57F13, 1957.

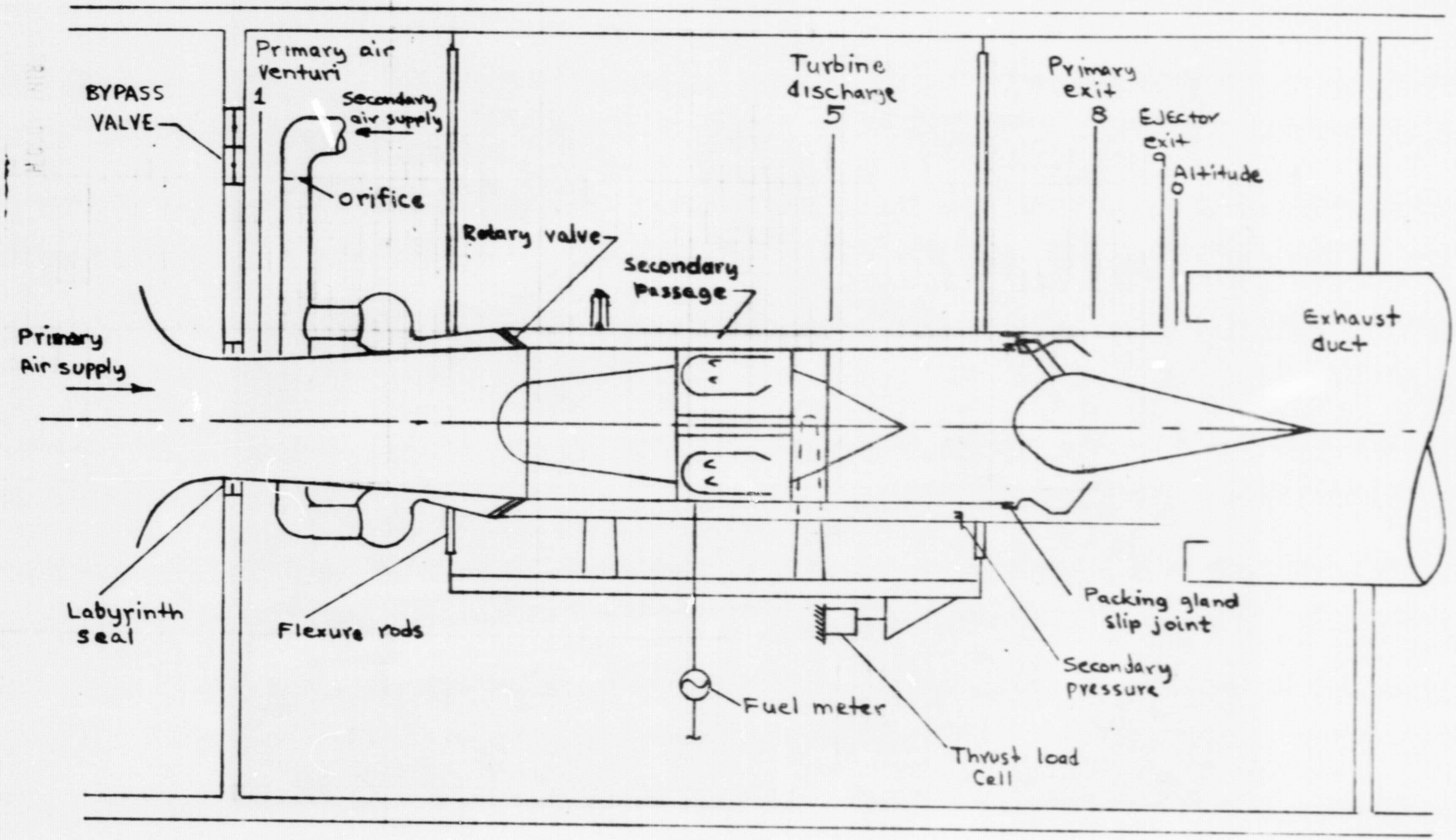

Figure 1.- Schematic of test installation.

C-68-2311

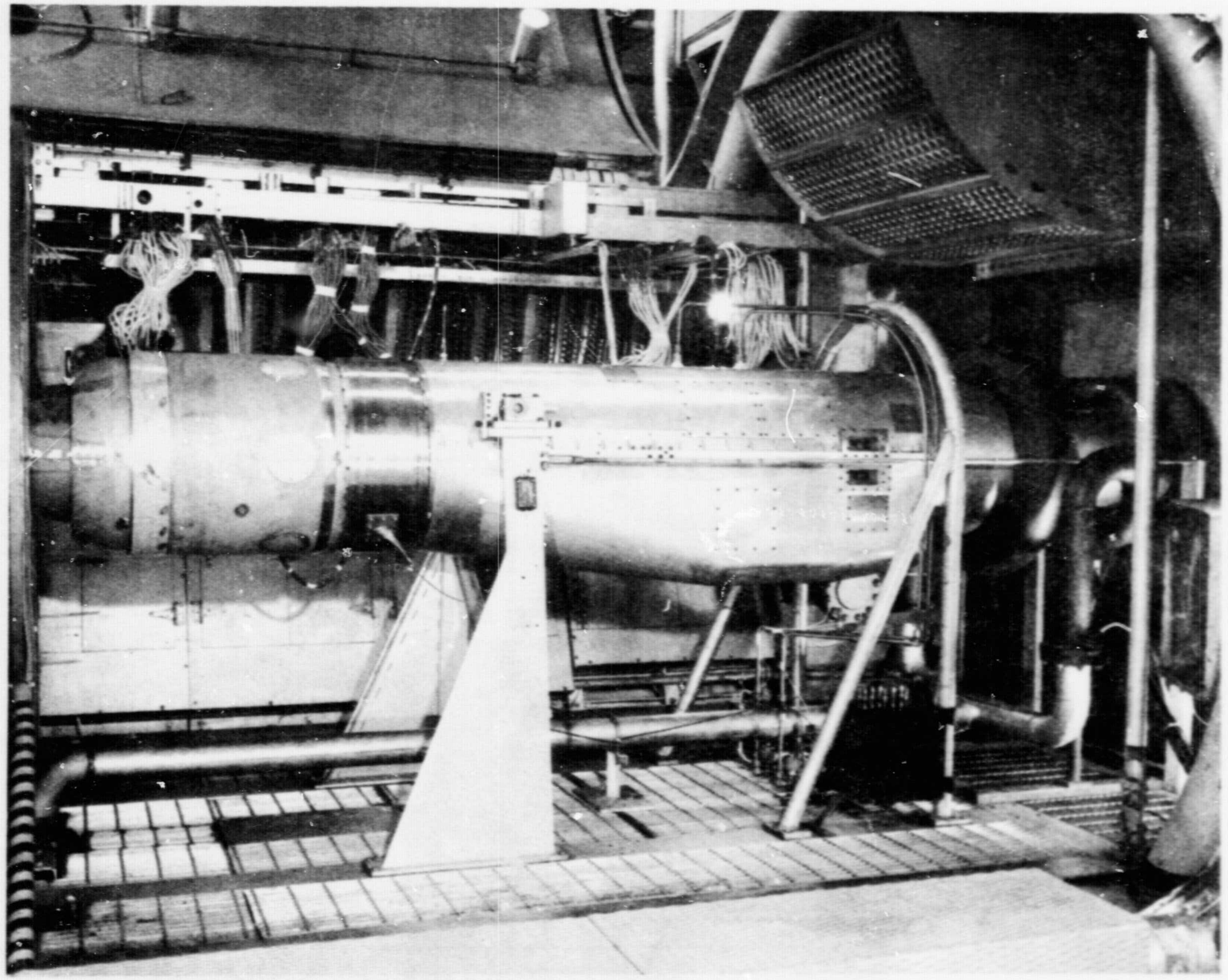

Figure 2.- Photograph of test installation.

C-68-2310

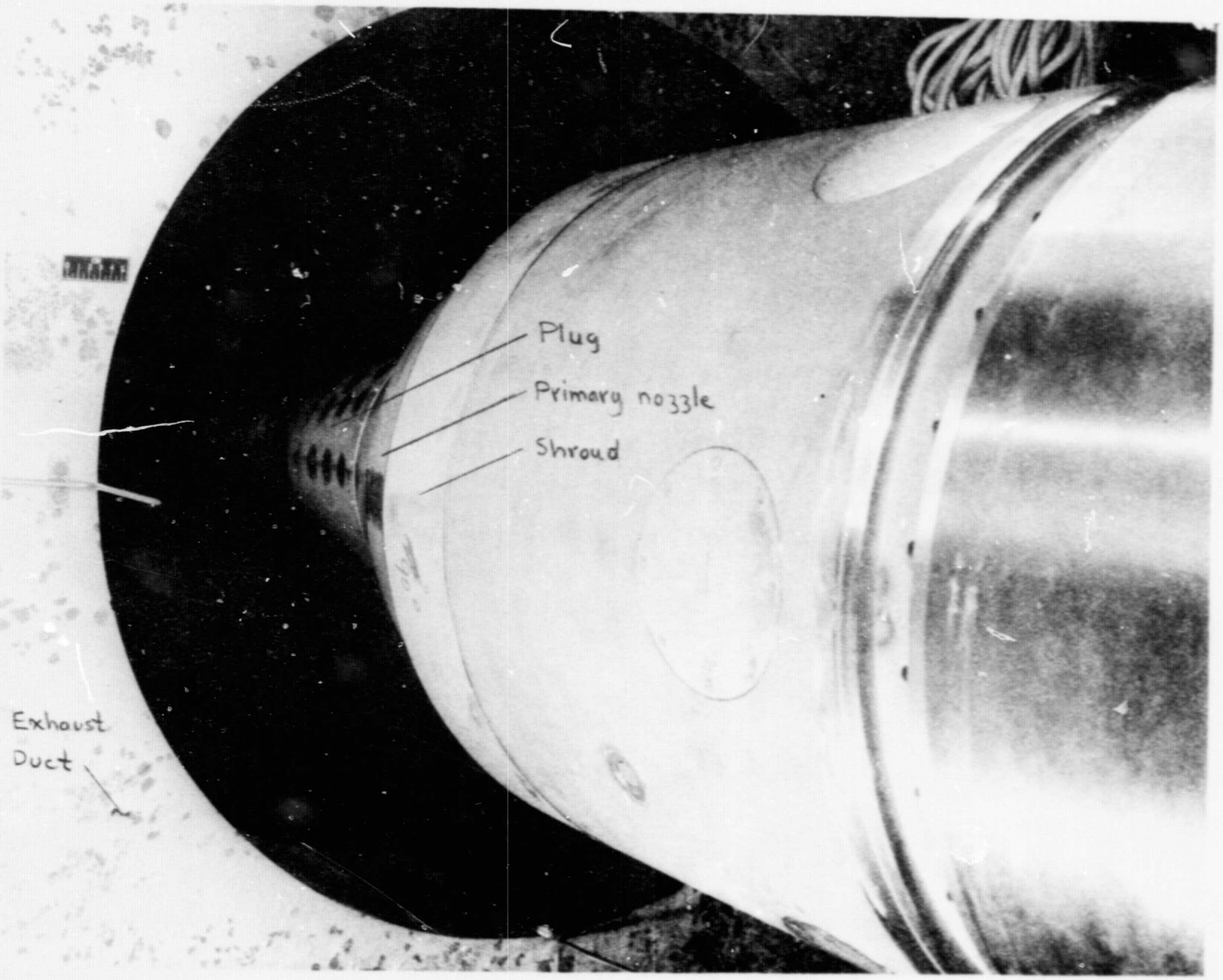

Figure 3.- Plug nozzle extending into exhaust duct.

C-68-1809

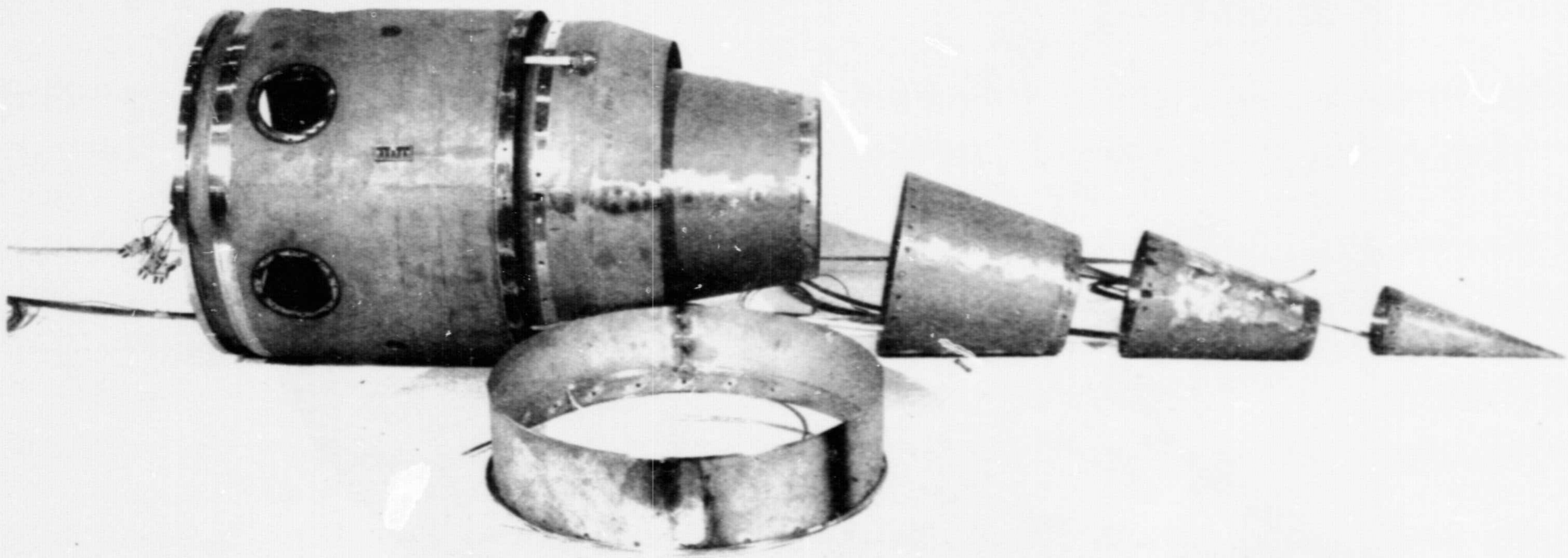

Figure 4. - View of expanded plug

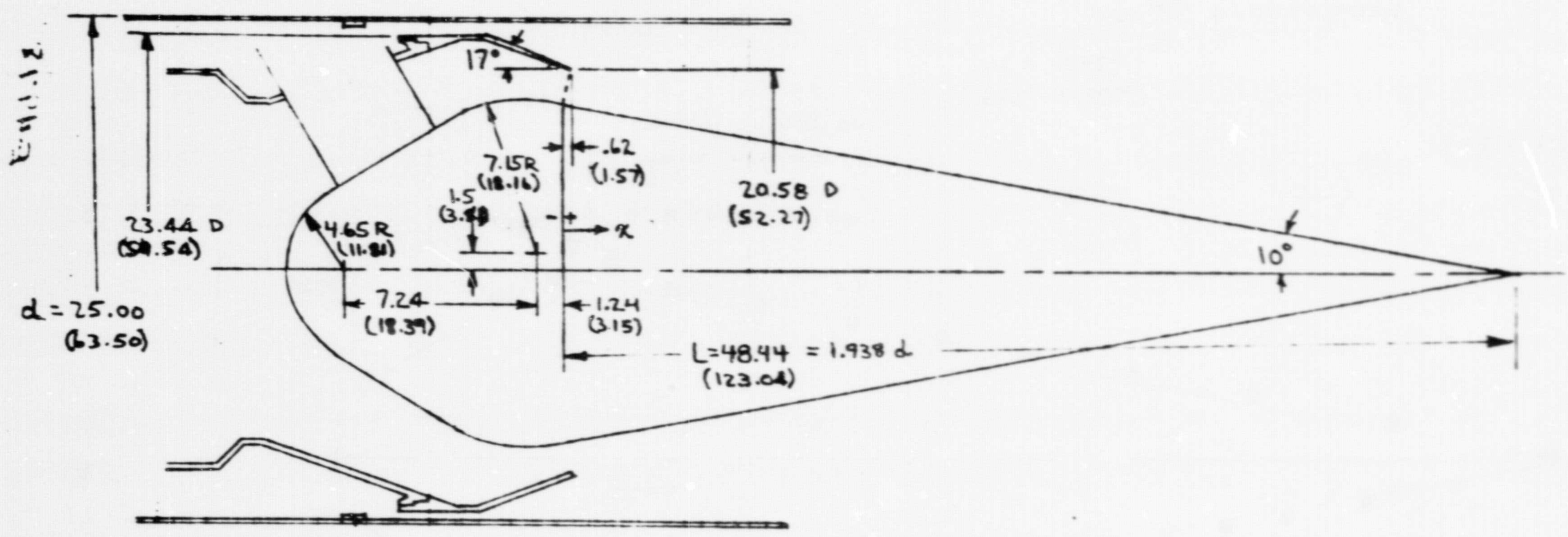

Figure 5.- Plug nozzle dimensions.
(All dimensions are in inches (cm) unless otherwise noted.)

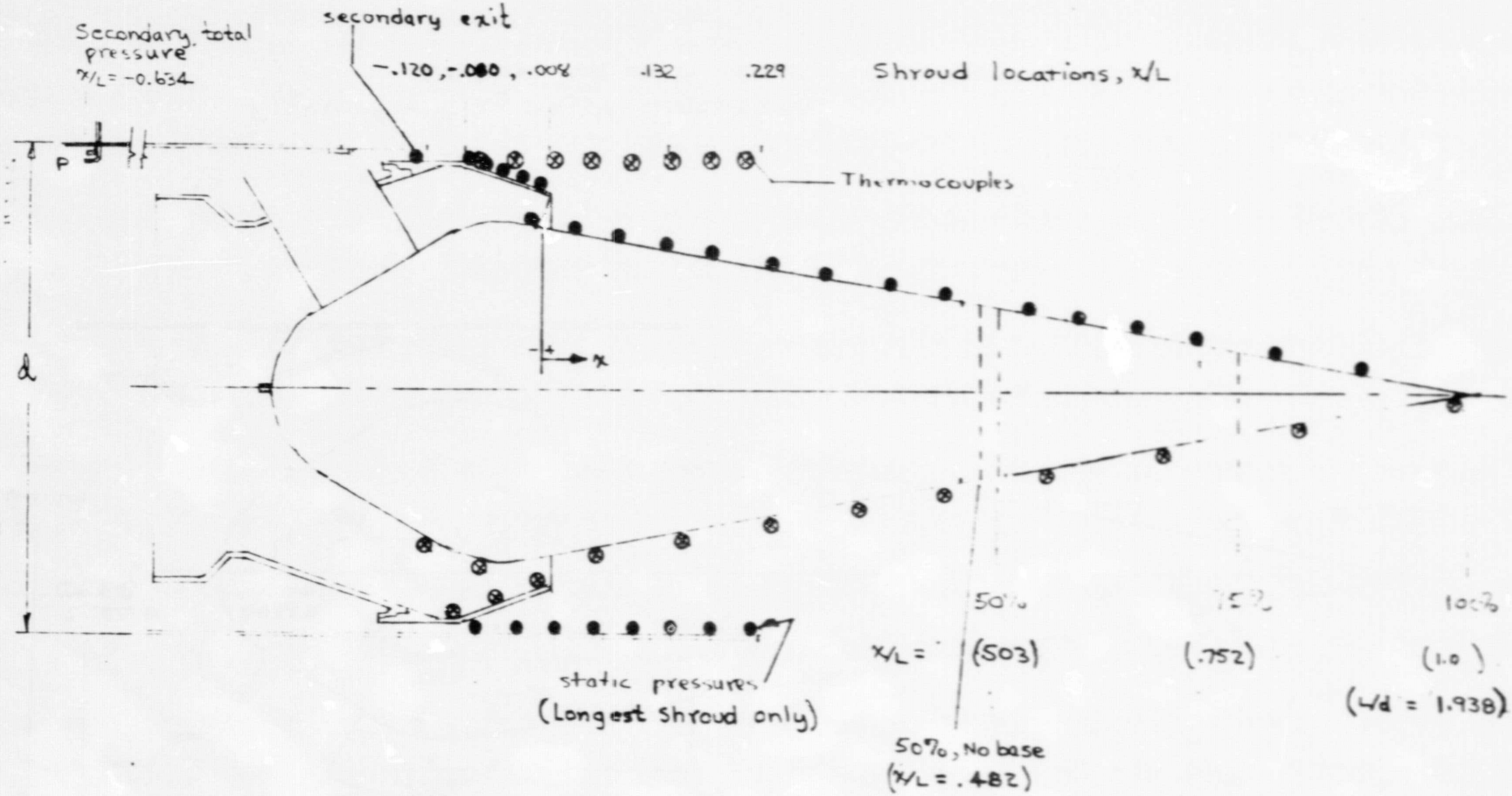

Plug truncations.

a) Shrouds & plug truncations.

Figure 6 . Plug nozzle instrumentation, shrouds, plug truncations.

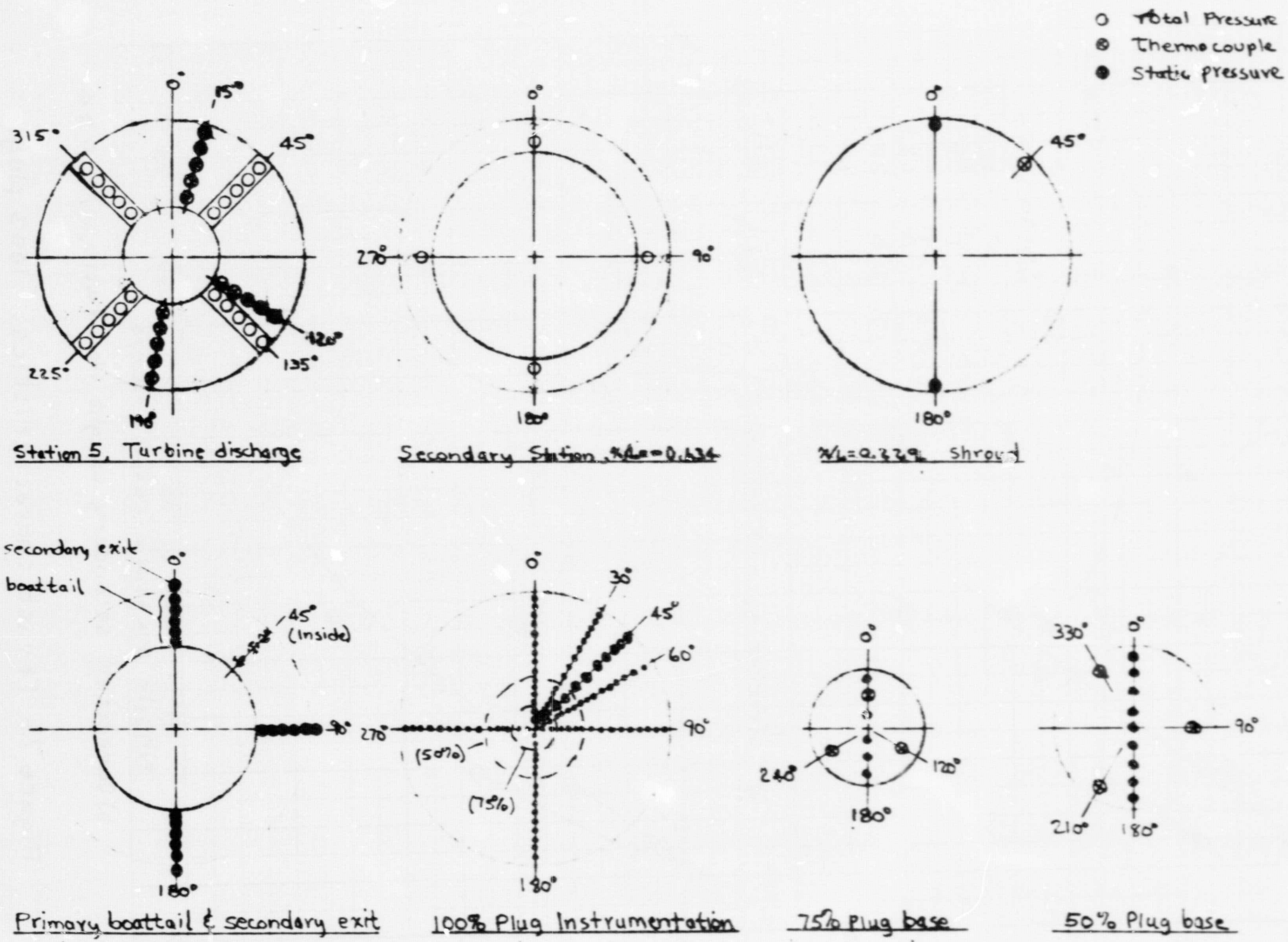

b.) Instrumentation. Looking upstream.

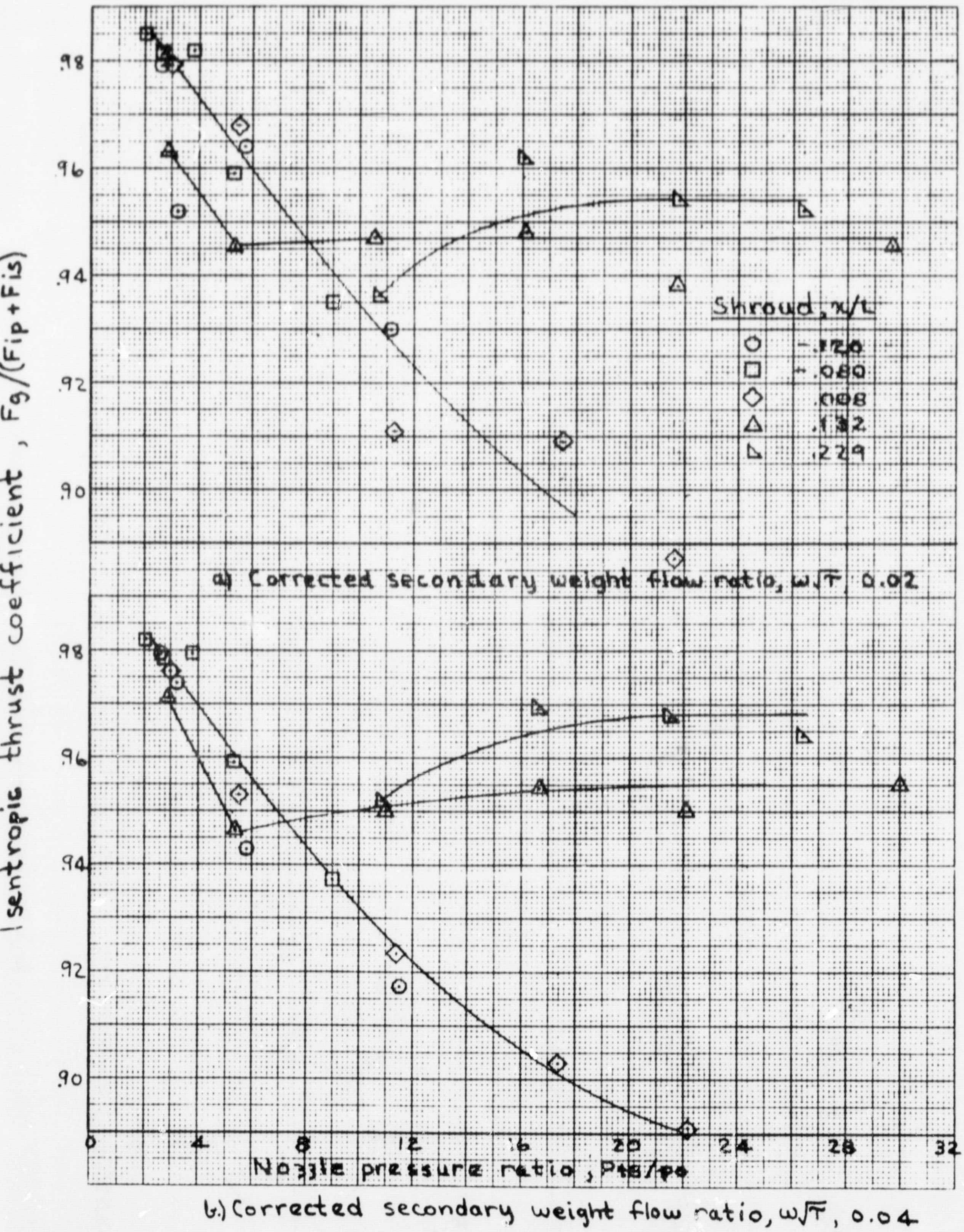

Figure 7.- Thrust characteristics. 100% plug.

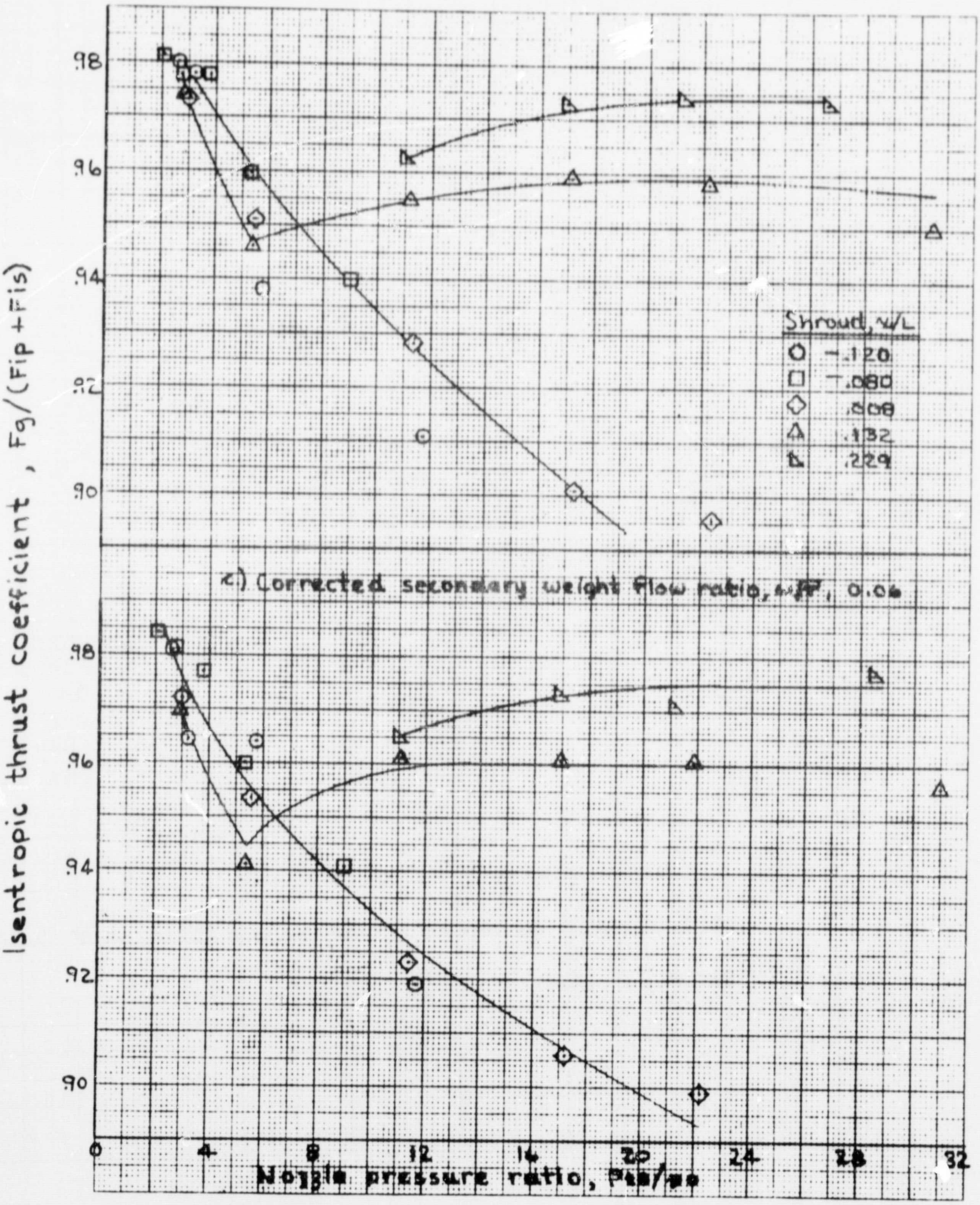

d.) Corrected secondary weight flow ratio, ω√T, 0.08

Figure 7.- (continued)

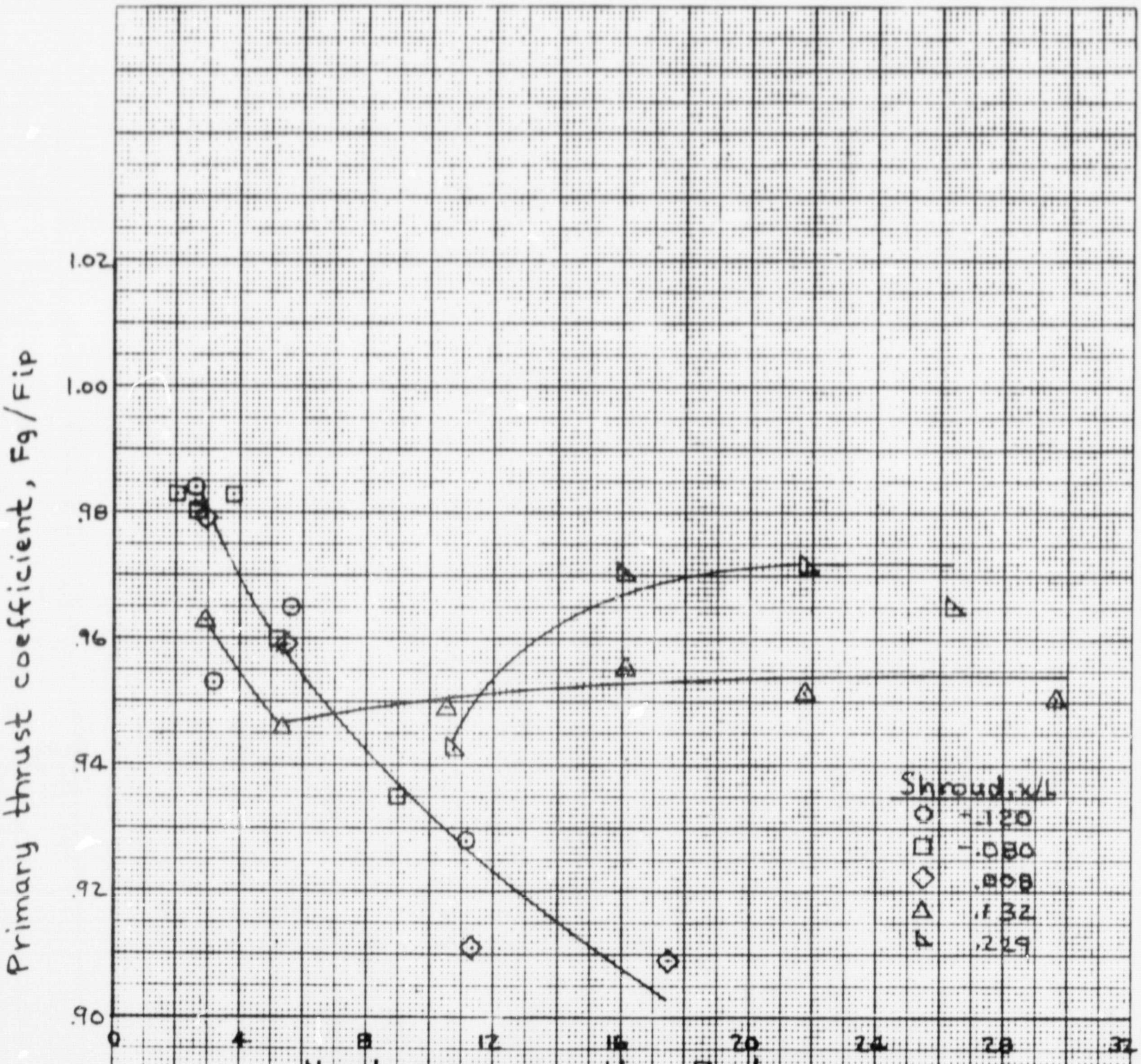

c) Corrected secondary weight flow ratio, ω√τ, 0.02

Figure 7.- (continued)

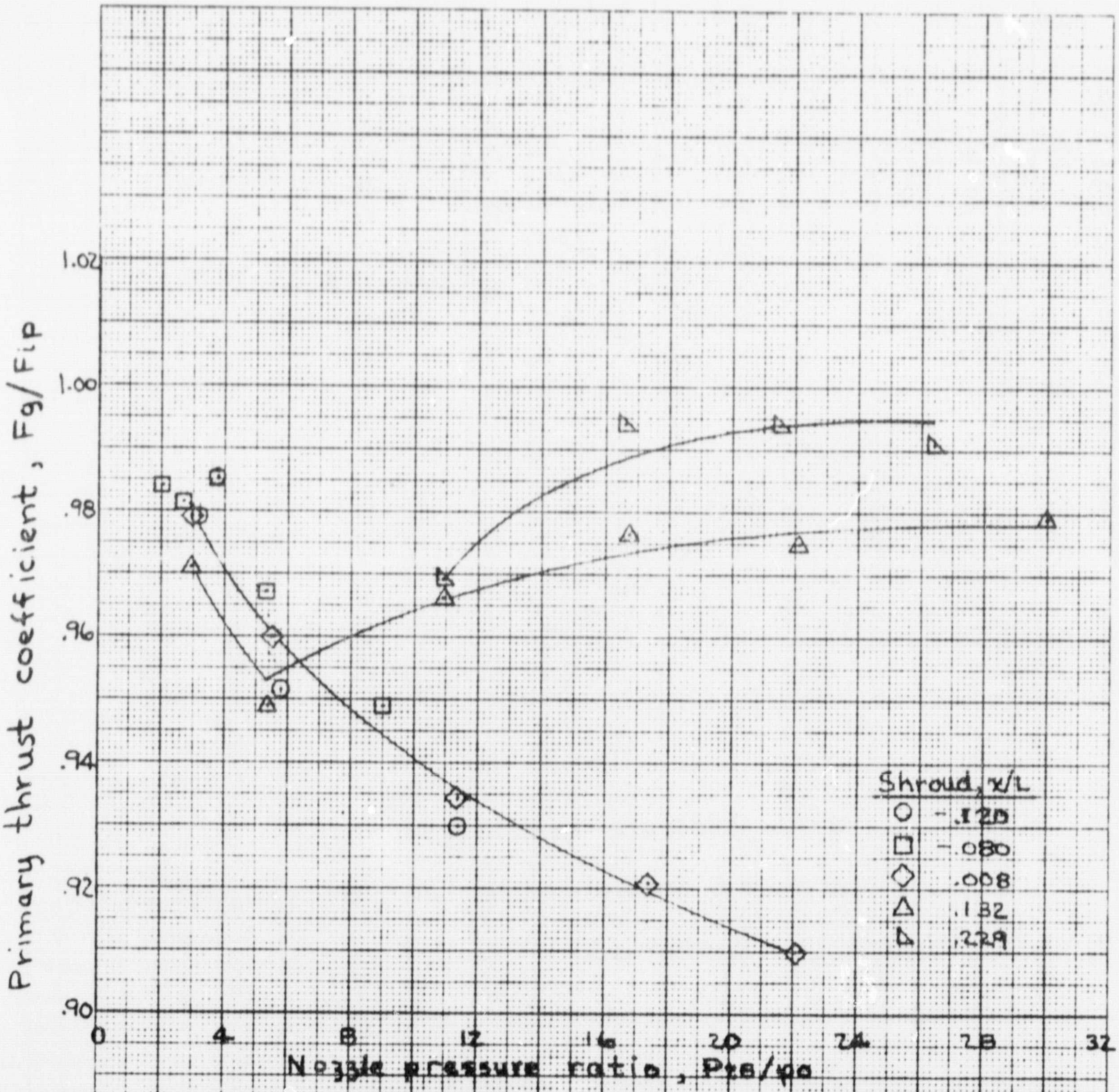

f.) Corrected secondary weight flow ratio, $\omega\sqrt{\tau}$, 0.04

Figure 7.- (continued)

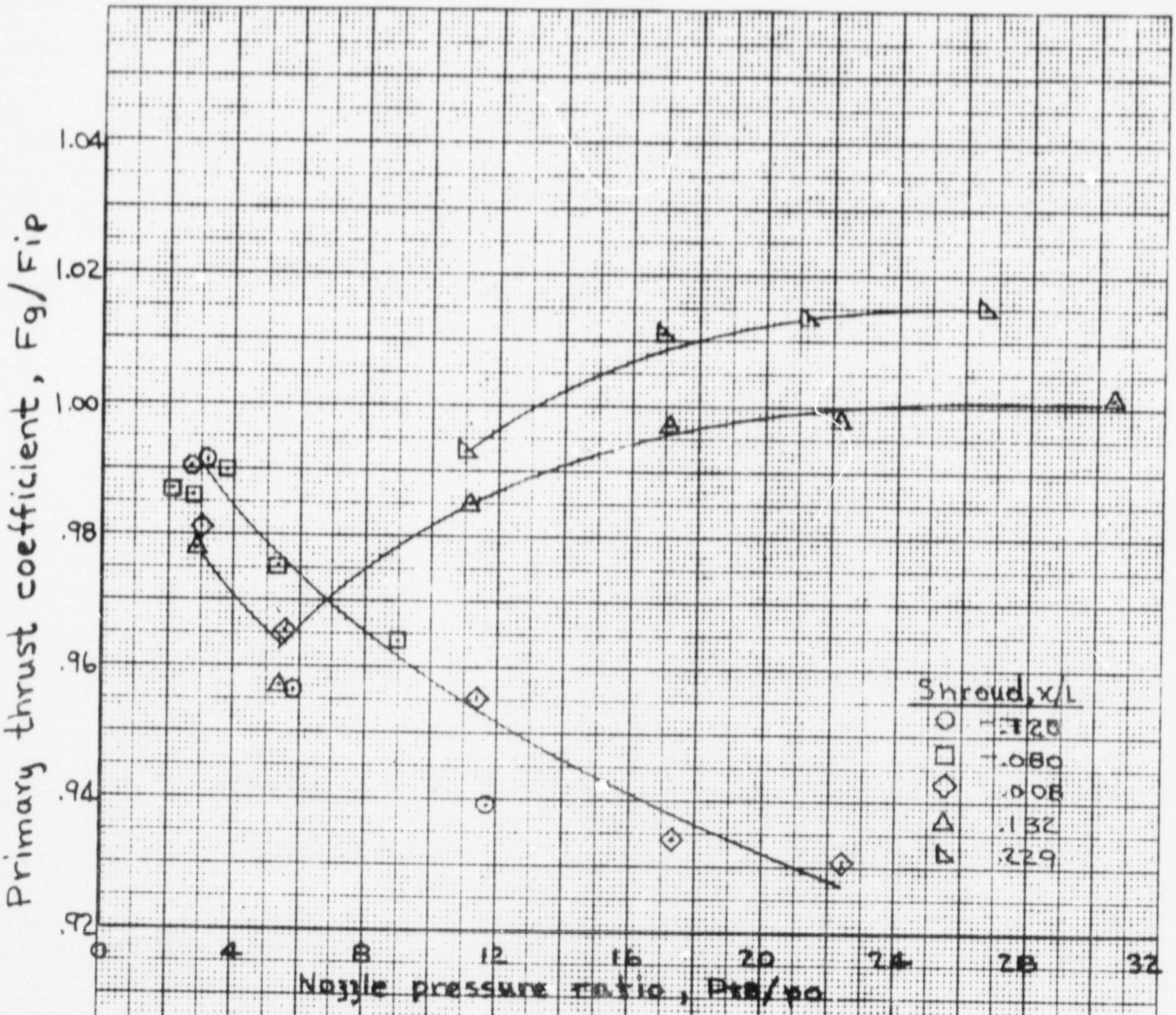

g) Corrected secondary weight flow ratio, $\omega\sqrt{\tau}$, 0.06

Figure 7.- (continued)

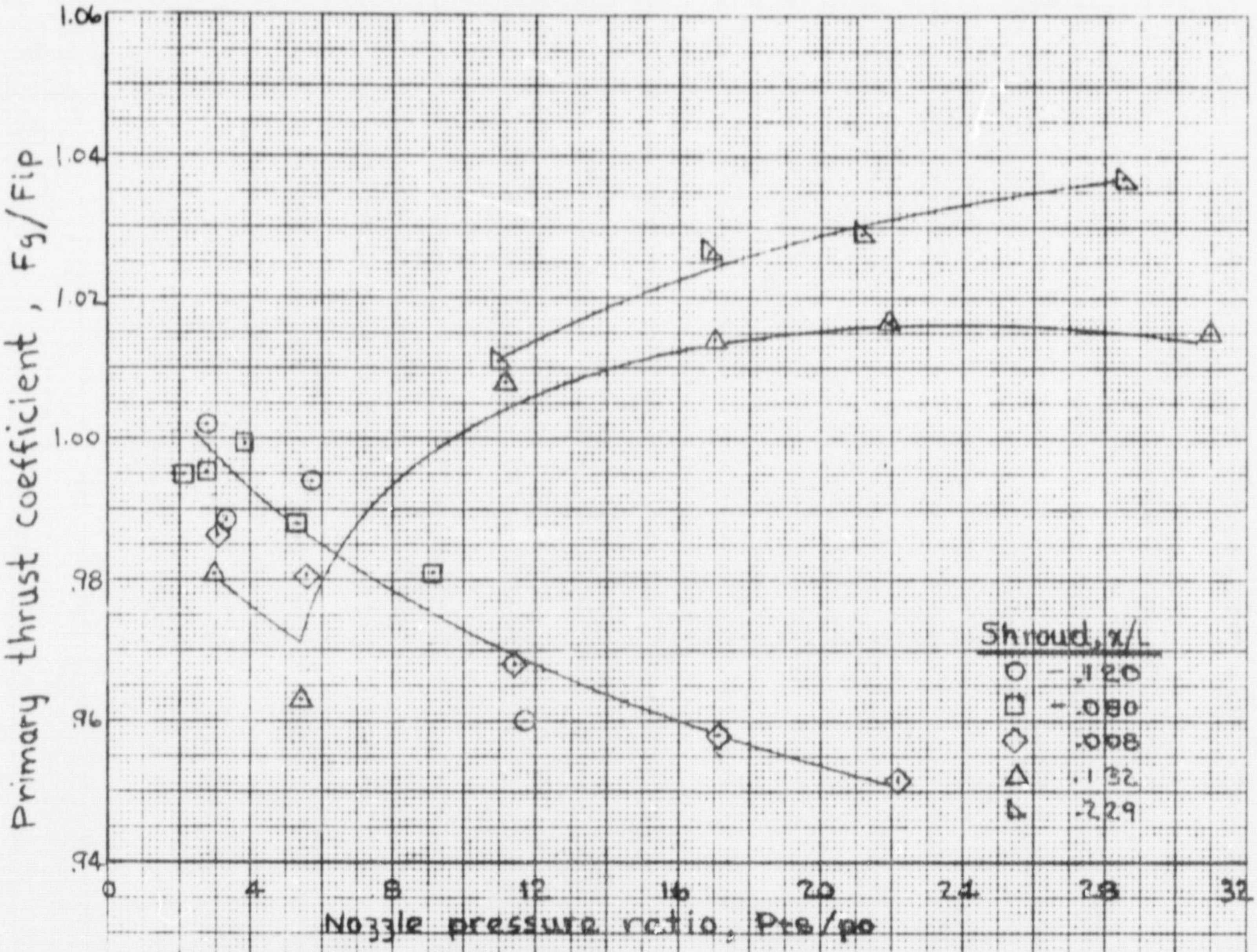

b) Corrected secondary weight flow ratio, ω√τ, 0.08

Figure 7.- (concluded)

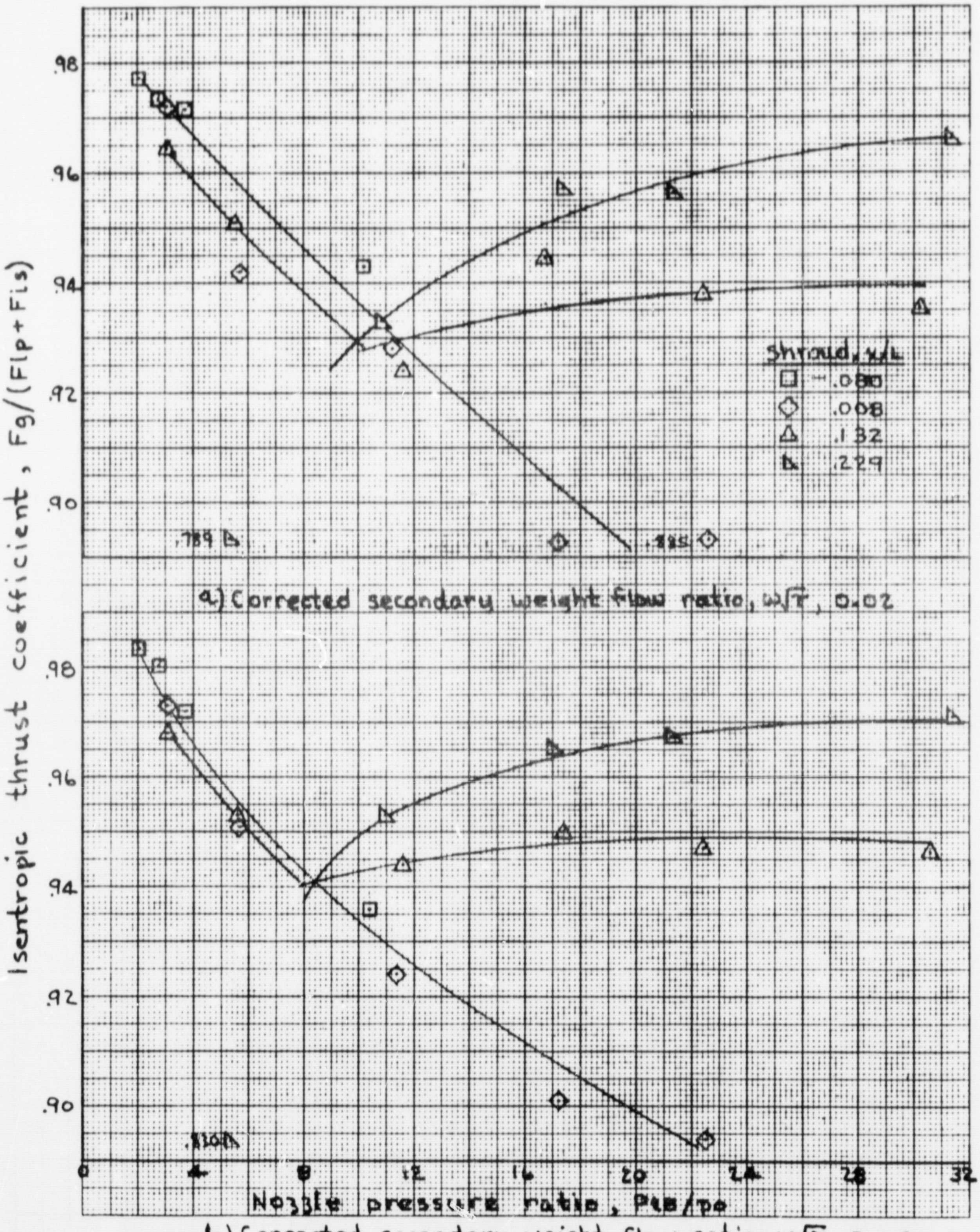

b.) Corrected secondary weight flow ratio, ω√τ, 0.04

Figure 8.- Thrust characteristics. 75 % plug.

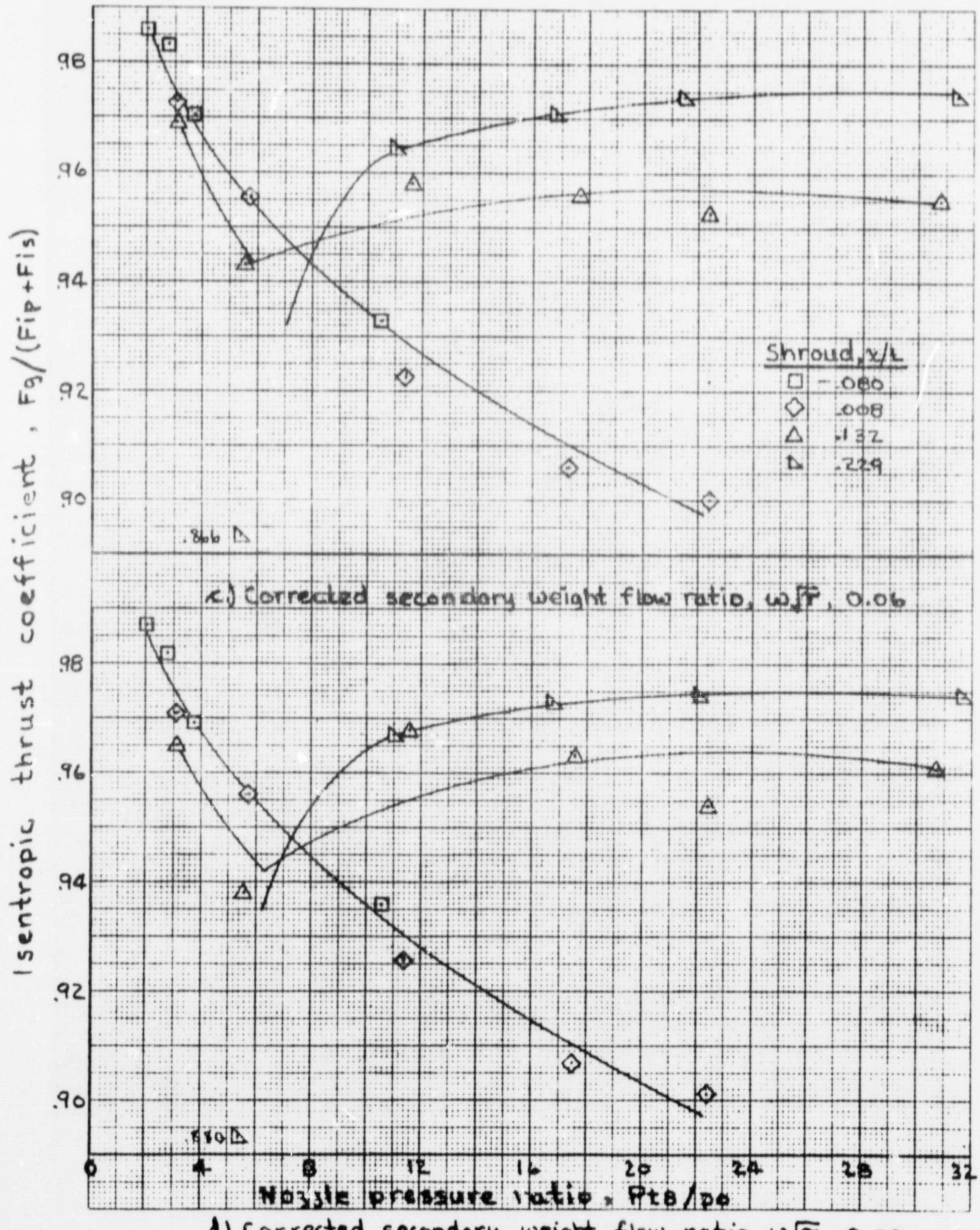

c.) Corrected secondary weight flow ratio, $\omega\sqrt{T}$, 0.06

d.) Corrected secondary weight flow ratio, $\omega\sqrt{T}$, 0.08

Figure 8.- (continued)

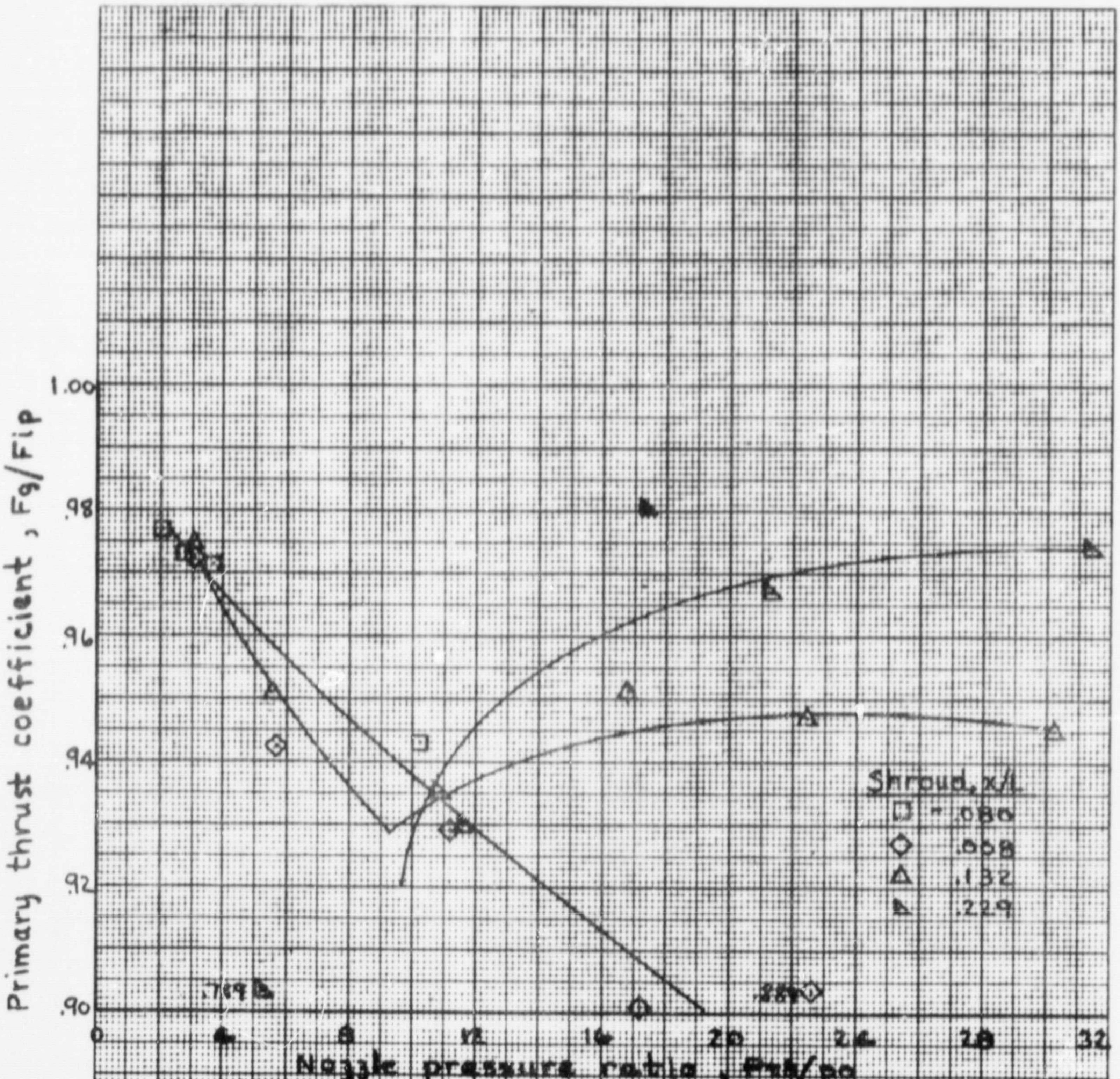

(b) Corrected secondary weight flow ratio, $\omega\sqrt{T}$, 0.02

Figure 8. - (continued)

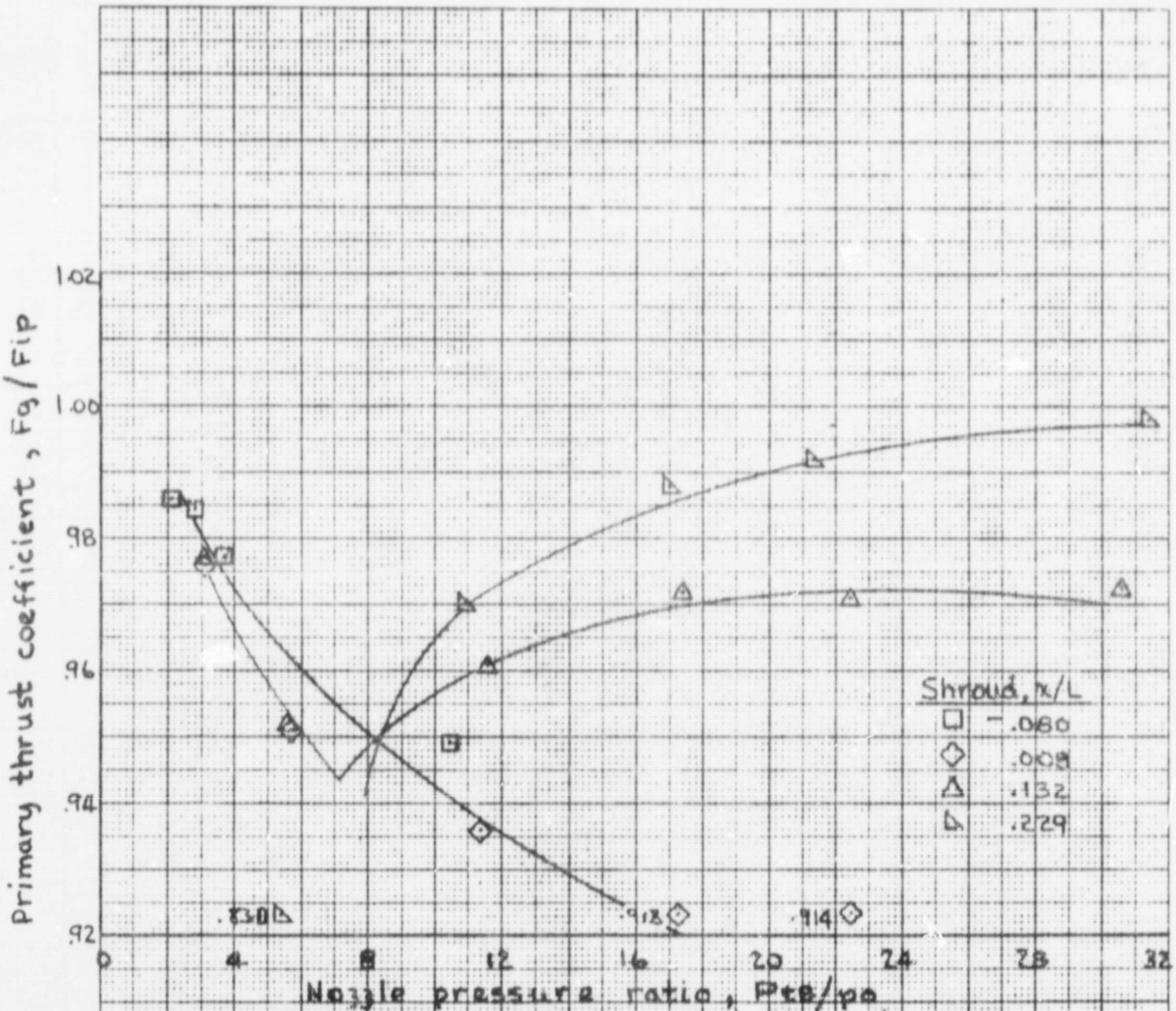

f) Corrected secondary weight flow ratio, ω√τ, 0.04

Figure 8.- (continued)

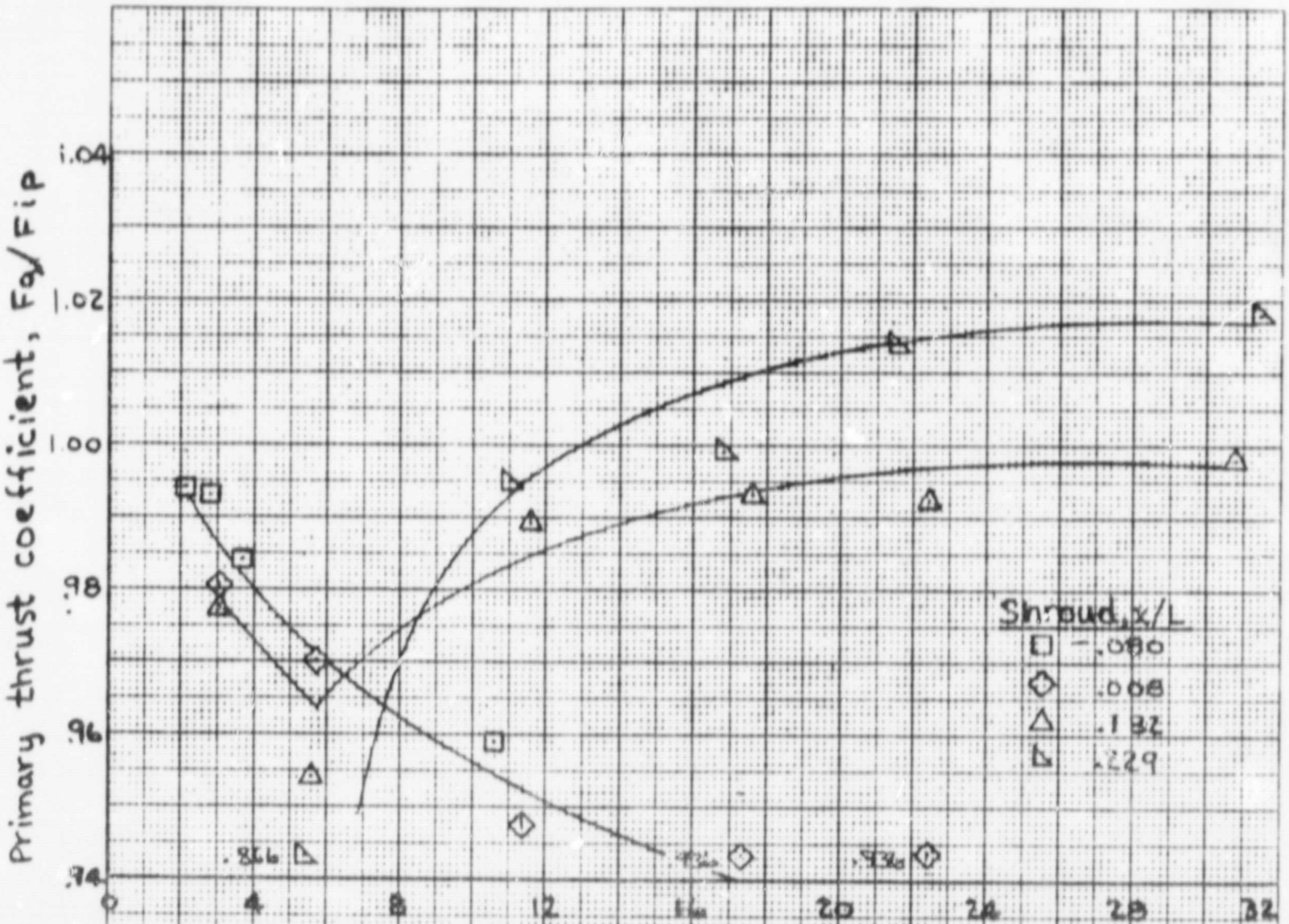

g) Corrected secondary weight flow ratio, $\omega\sqrt{\tau}$, 0.06

Figure 8. - (continued)

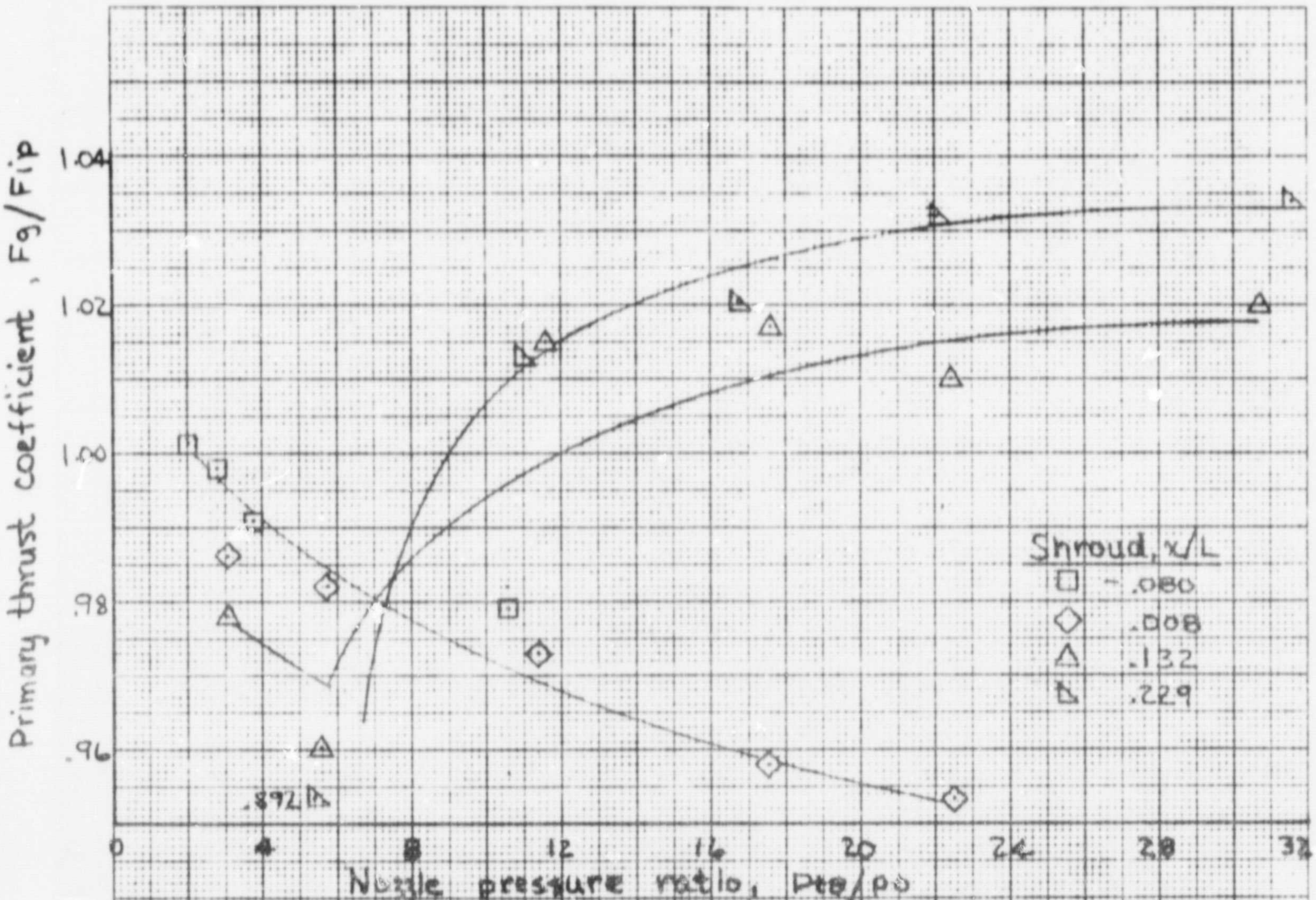

h) Corrected secondary weight flow ratio, $\omega\sqrt{T}$, 0.08

Figure 8.- (Concluded)

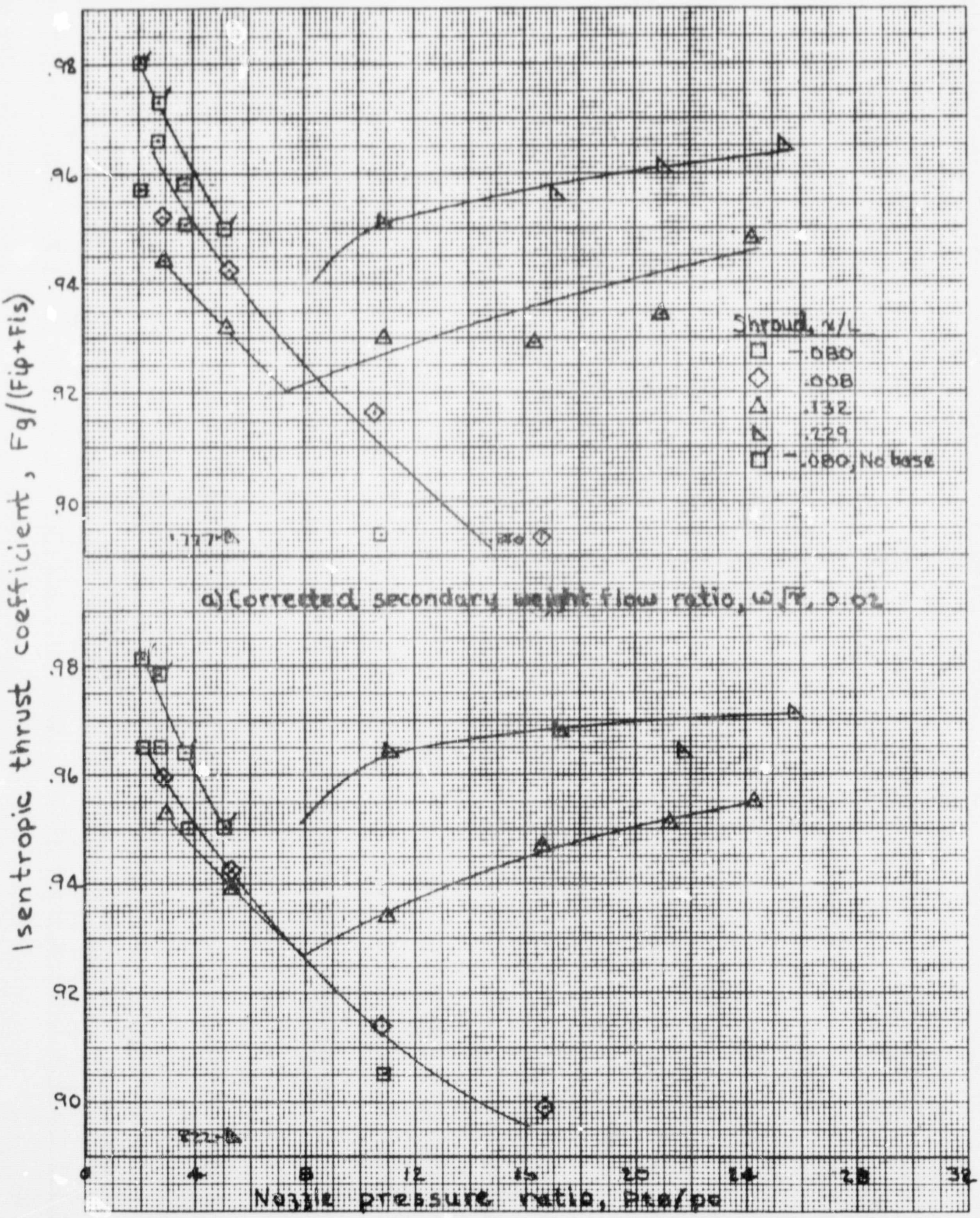

b) Corrected secondary weight flow ratio, ω√T, 0.04

Figure 9.- Thrust characteristics. 50% plug.

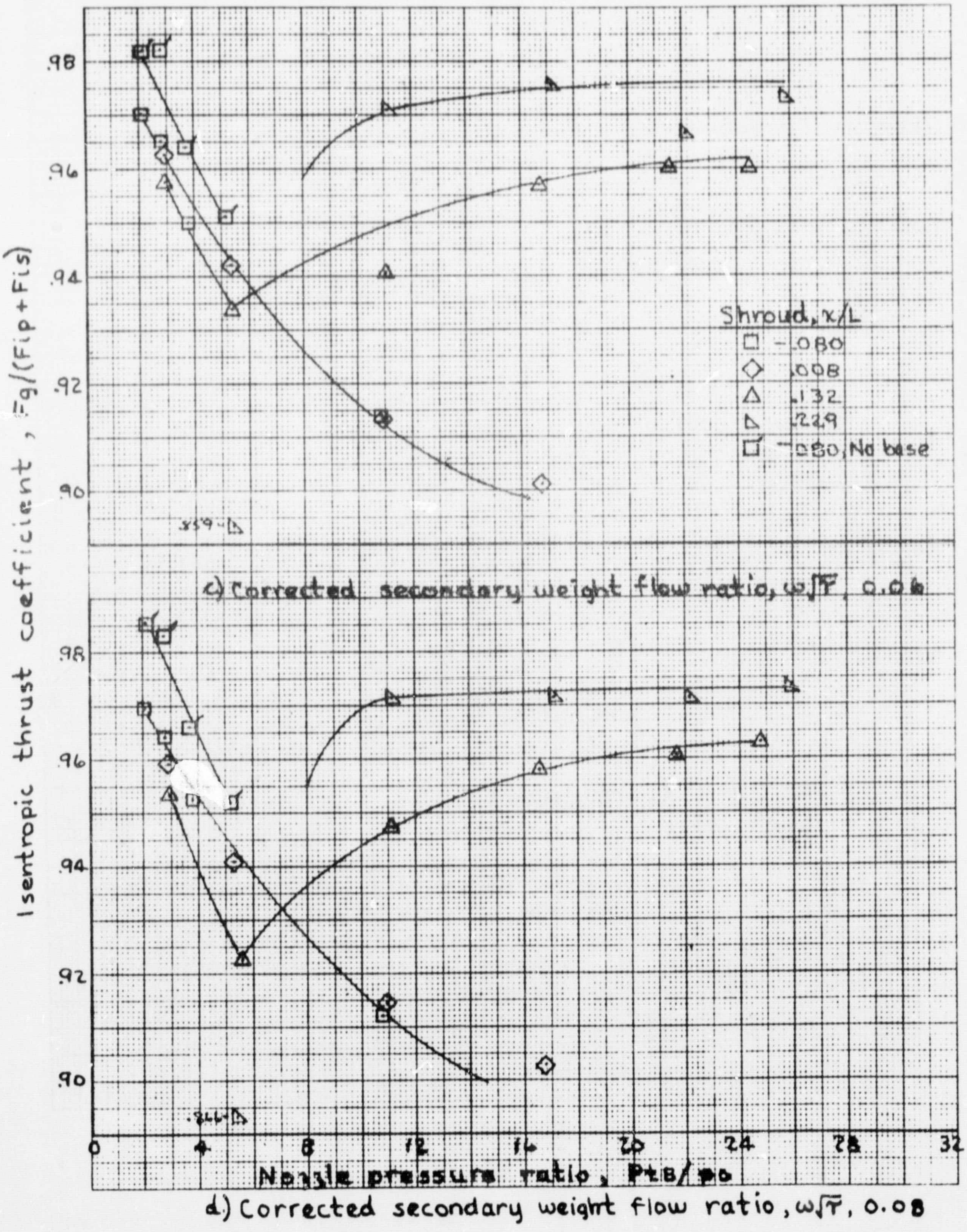

d.) Corrected secondary weight flow ratio, ω√T, 0.08

Figure 9.- (continued)

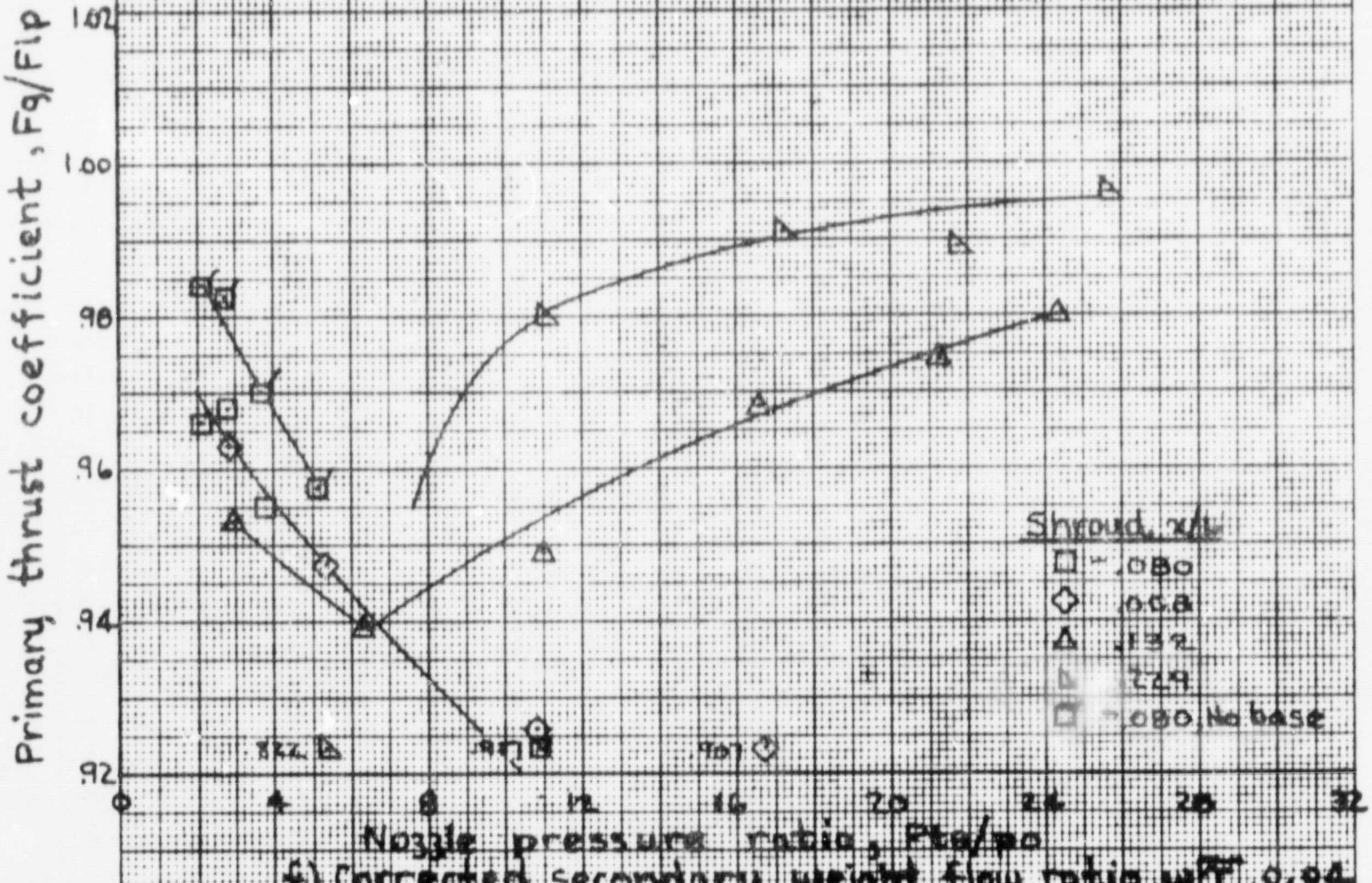

f) Corrected secondary weight flow ratio, ω√τ, 0.04

Figure 9.- (Continued)

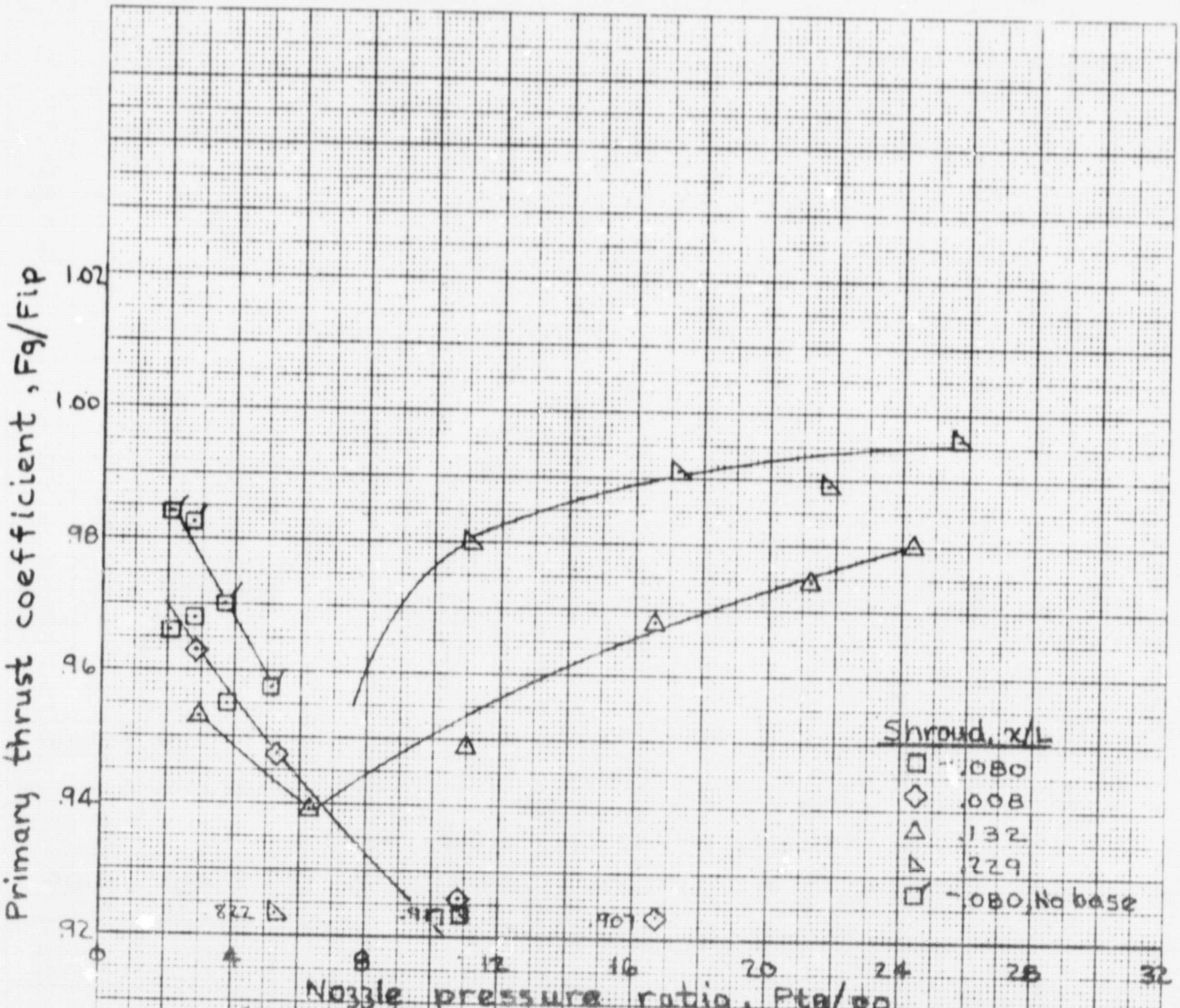

f.) Corrected secondary weight flow ratio, $\omega\sqrt{\tau}$, 0.04

Figure 9.- (Continued)

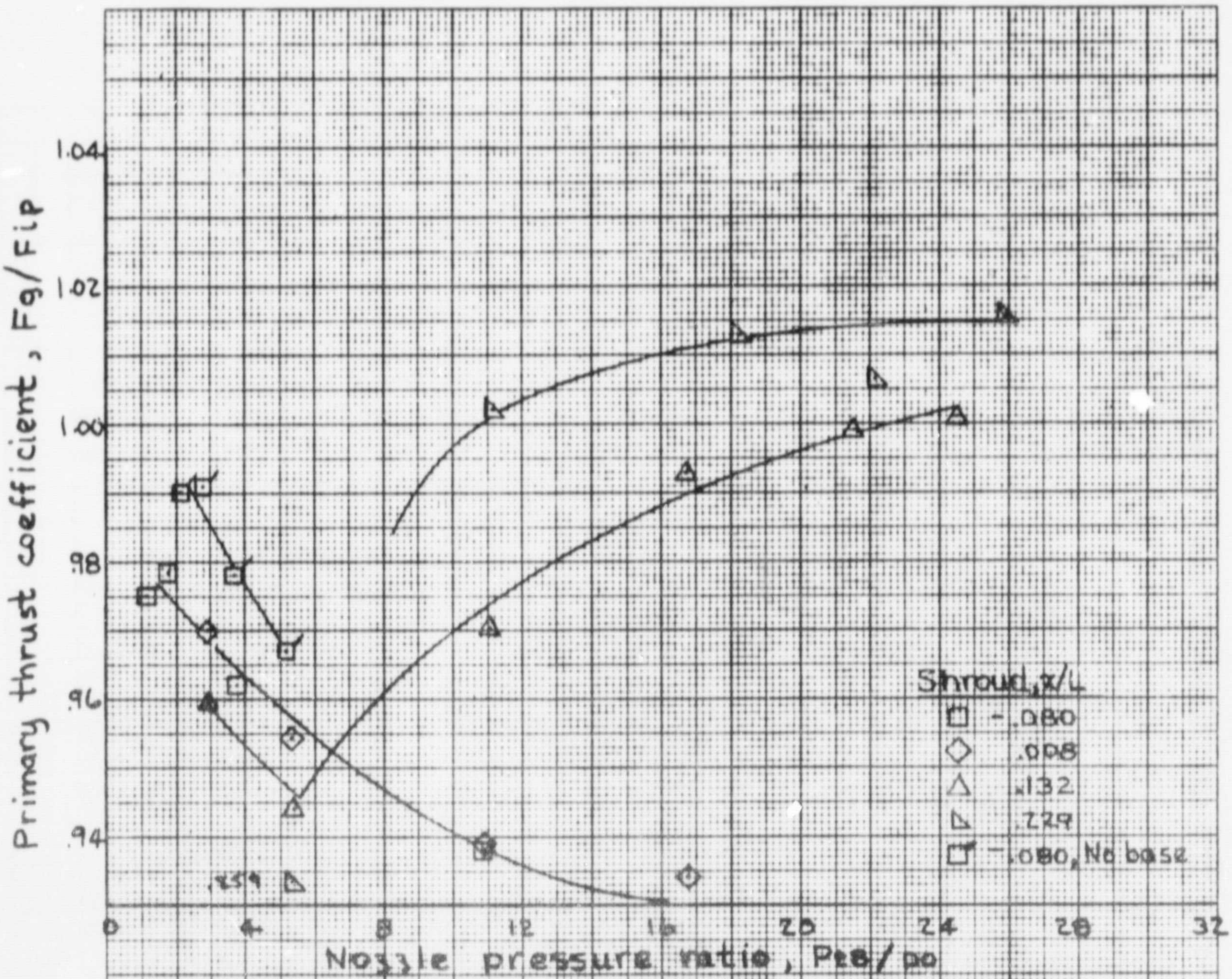

g.) Corrected secondary weight flow ratio, $\omega\sqrt{\tau}$, 0.06

Figure 9.- (continued)

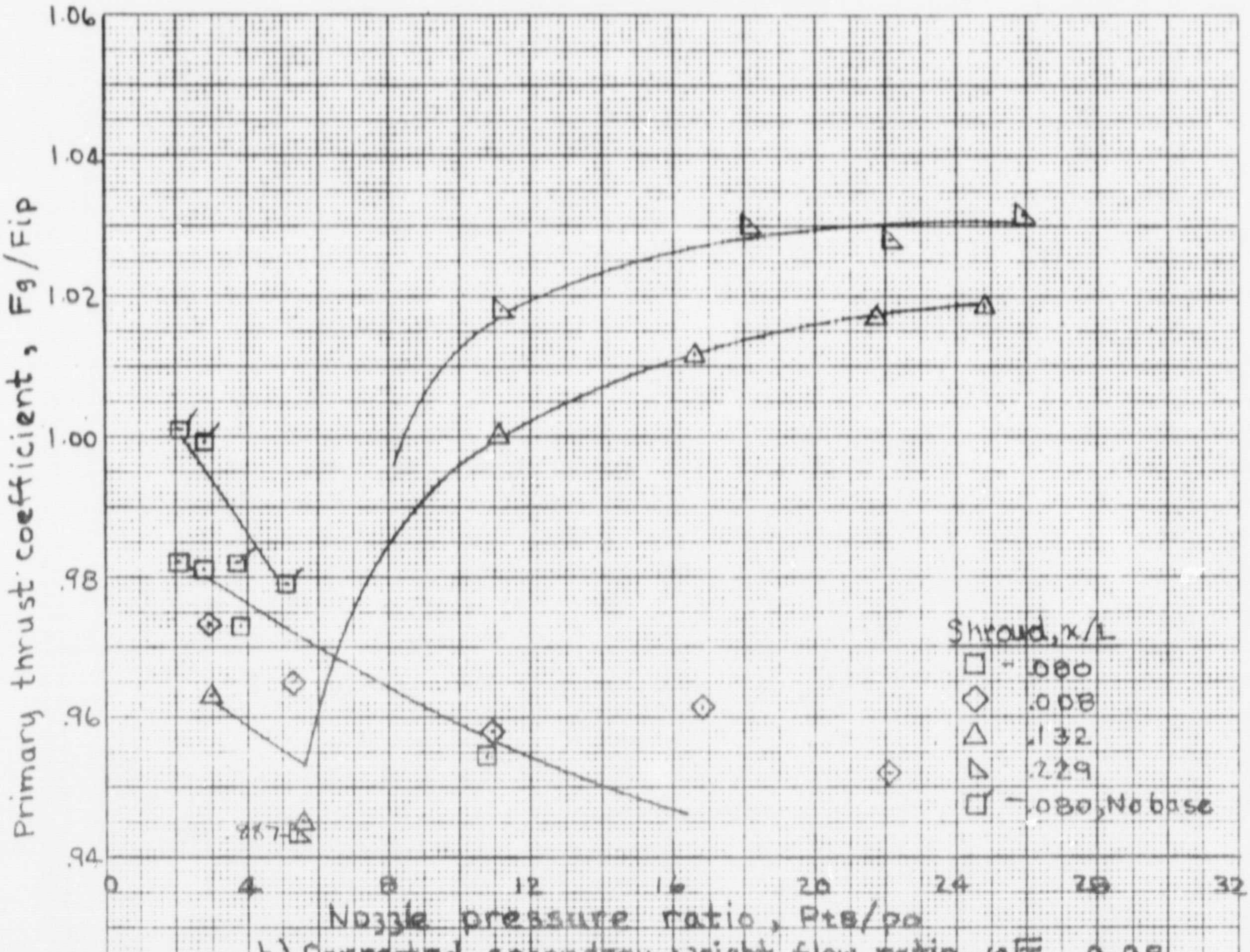

Nozzle pressure ratio, Pt8/po

h) Corrected secondary weight flow ratio, $\omega\sqrt{\tau}$, 0.08

Figure 9.- (concluded)

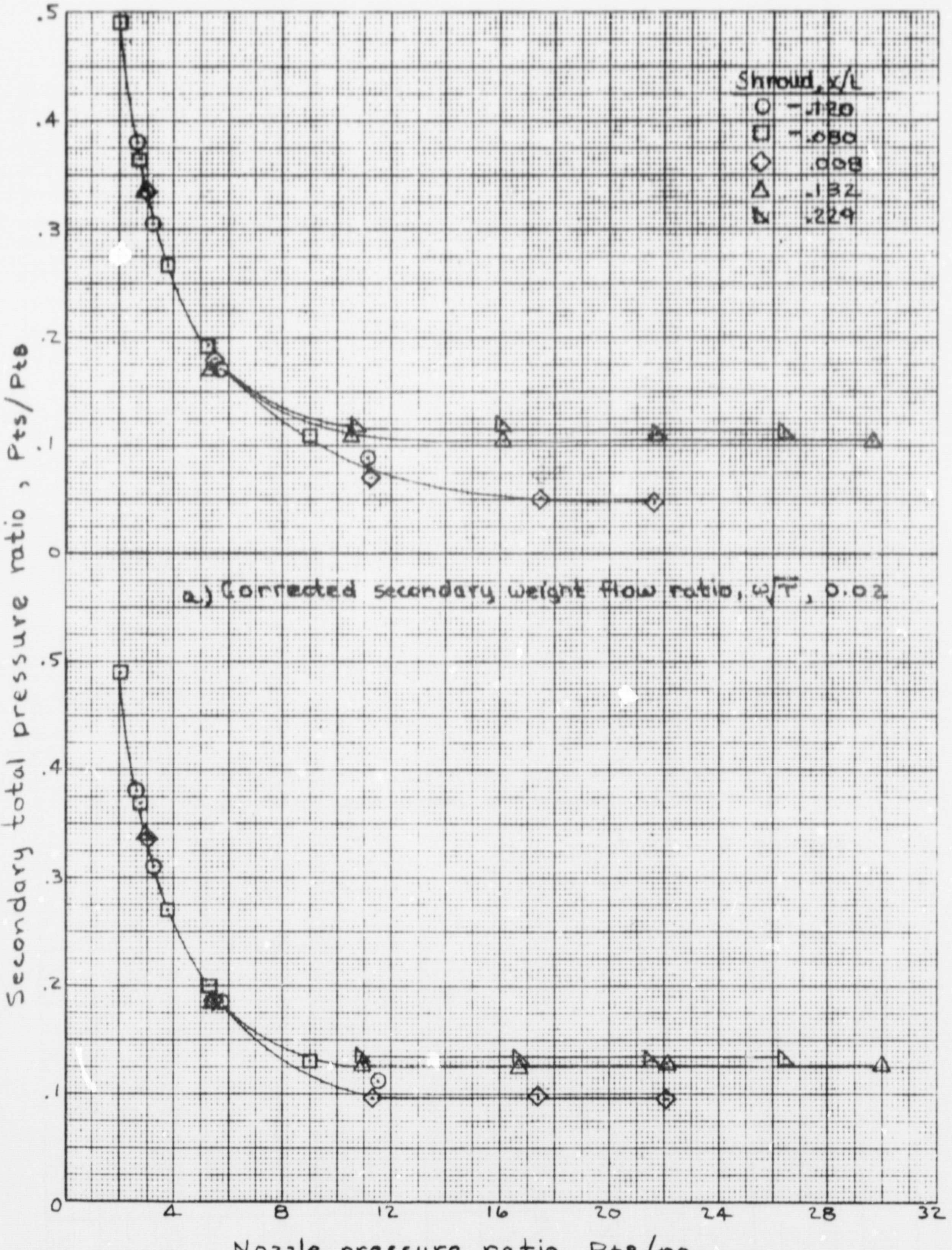

b.) Corrected secondary weight flow ratio, ω√T, 0.04

Figure 10.- Pumping characteristics. 100% plug.

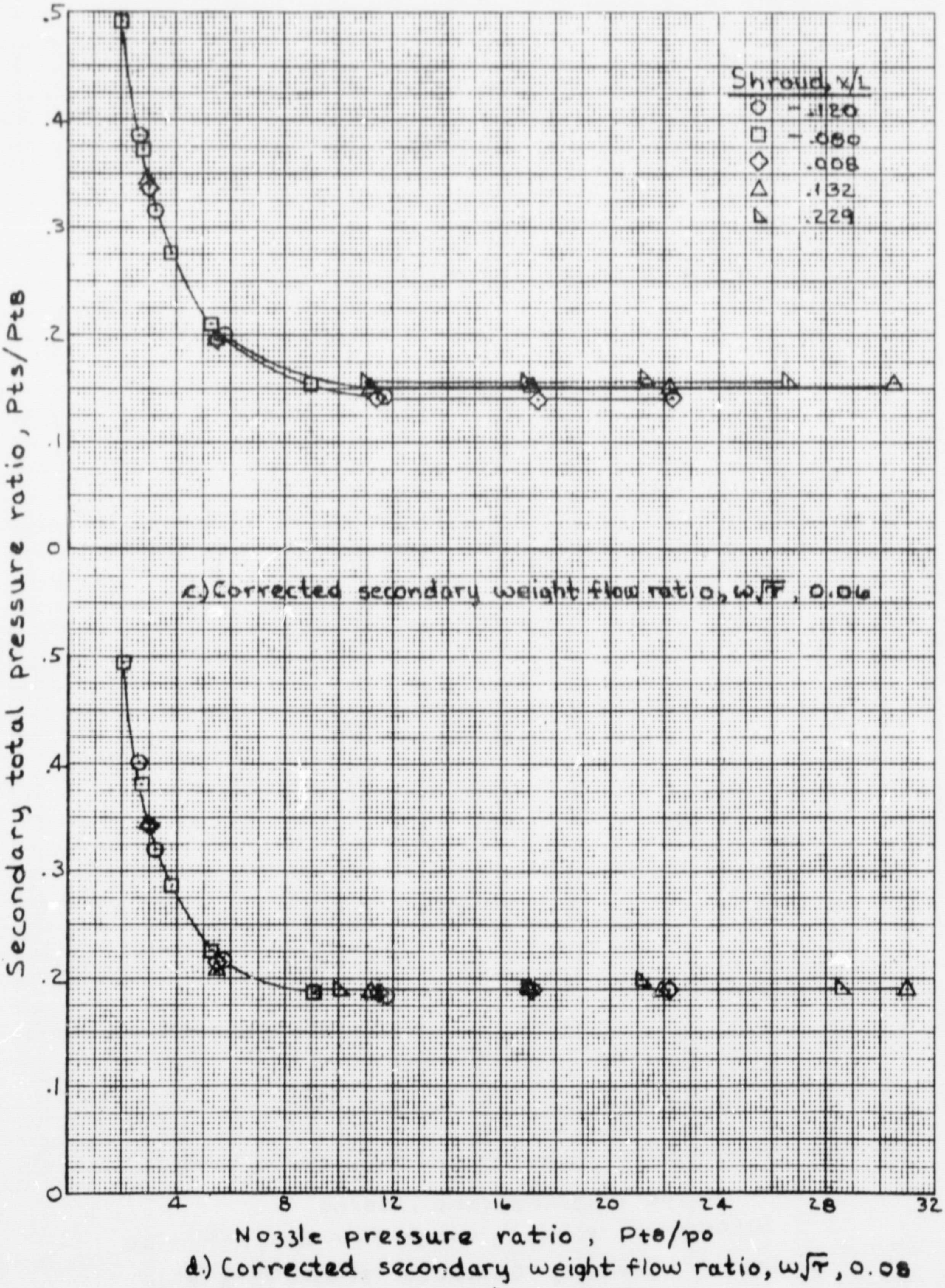

d.) Corrected secondary weight flow ratio, $\omega\sqrt{\tau}$, 0.08

Figure 10.- (concluded)

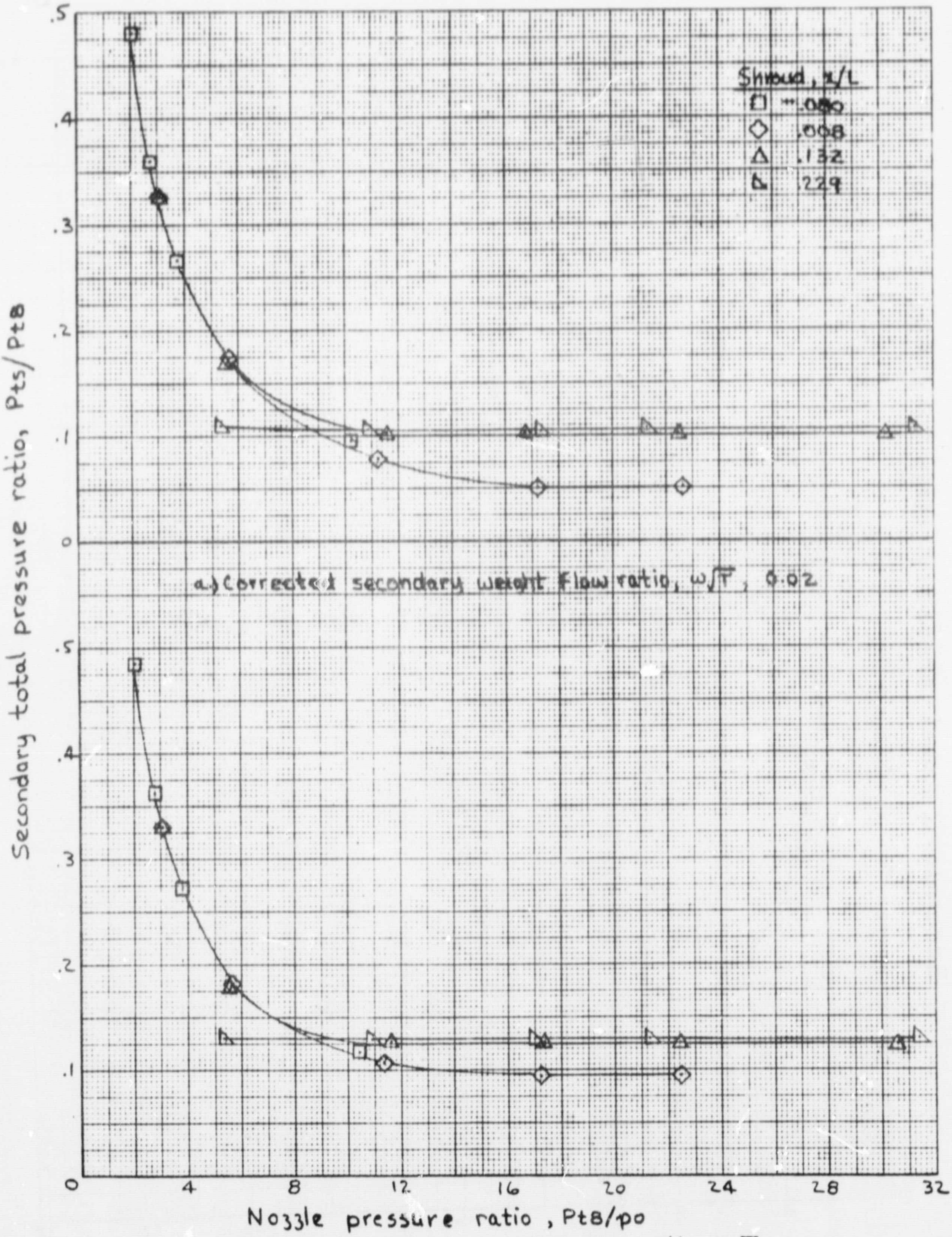

b.) Corrected secondary weight flow ratio, $\omega\sqrt{T}$, 0.04

Figure 11.- Pumping characteristics. 75% plug.

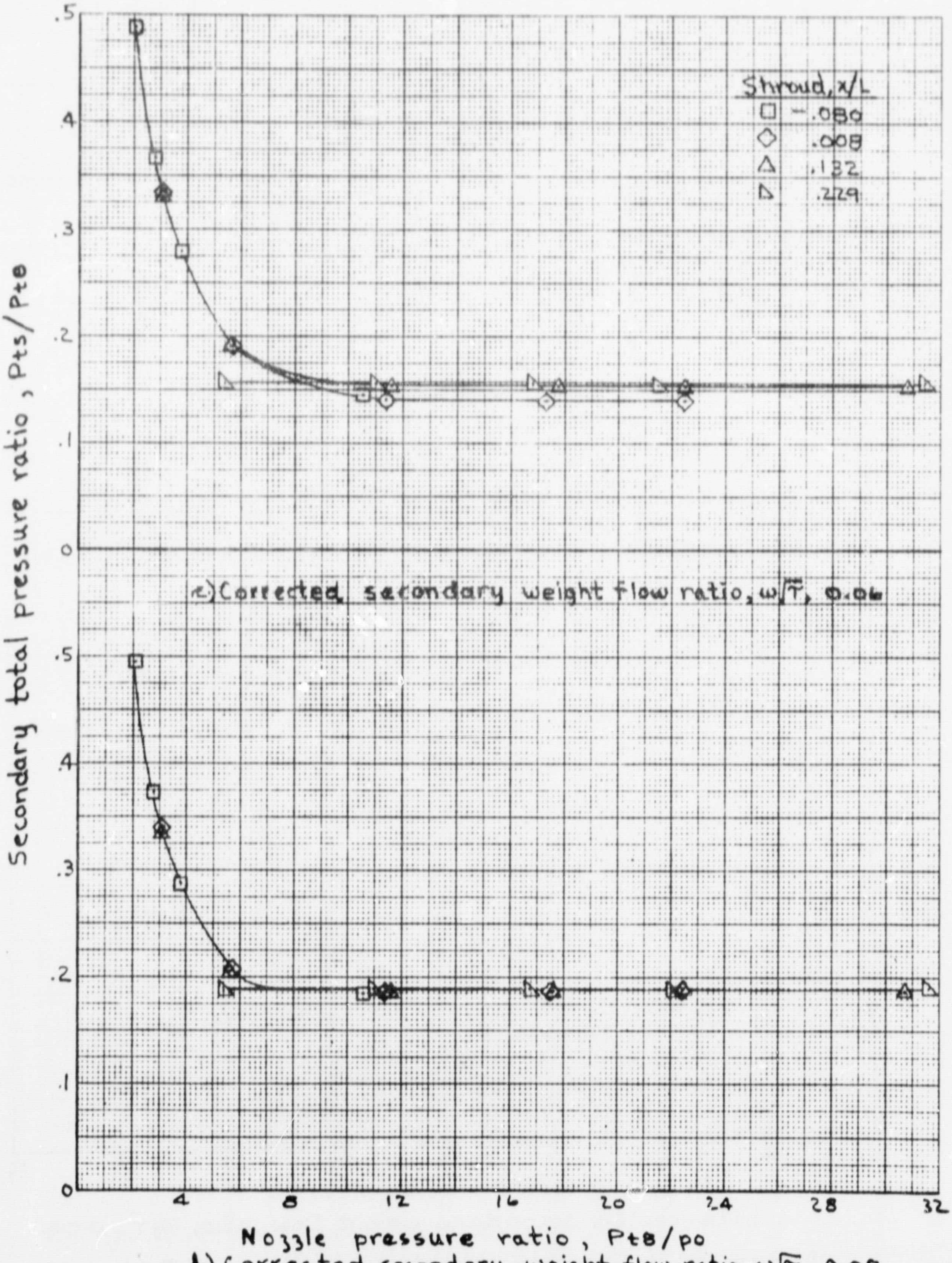

d.) Corrected secondary weight flow ratio, ω√τ, 0.08

Figure 11.- (concluded)

E-1994

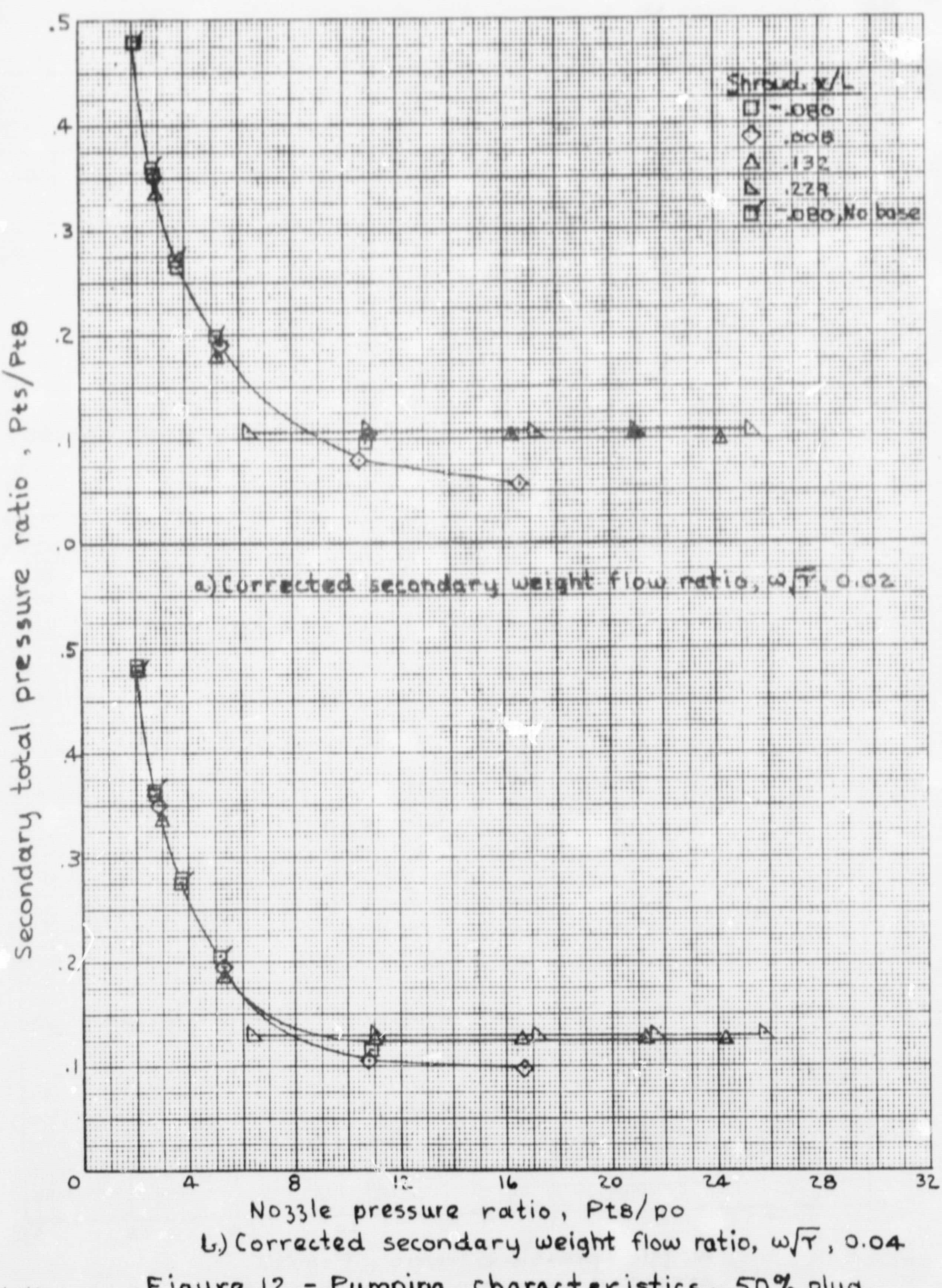

b) Corrected secondary weight flow ratio, $\omega\sqrt{T}$, 0.04

Figure 12.- Pumping characteristics. 50% plug.

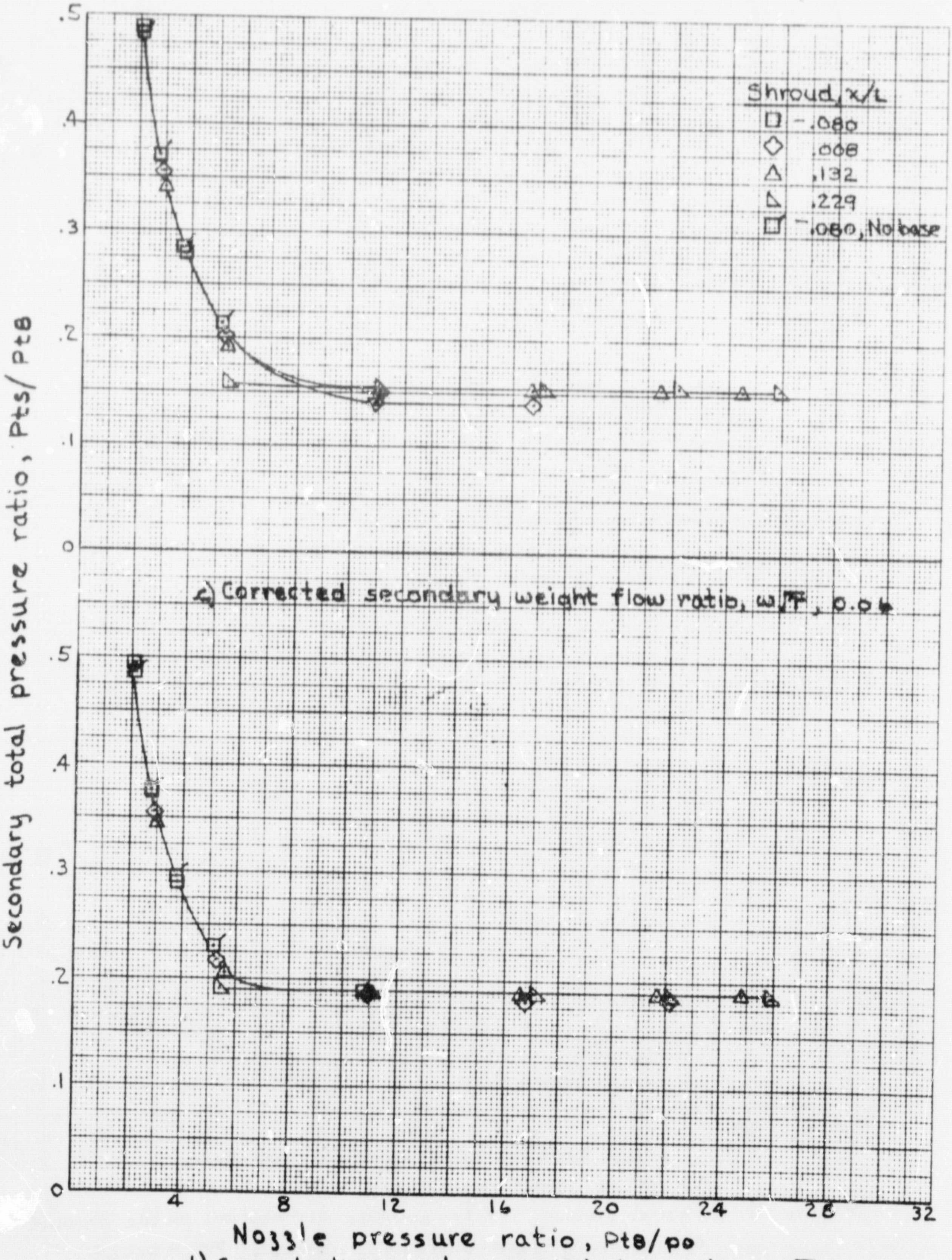

d) Corrected secondary weight flow ratio, ω√T, 0.08

Figure 12.- (concluded)

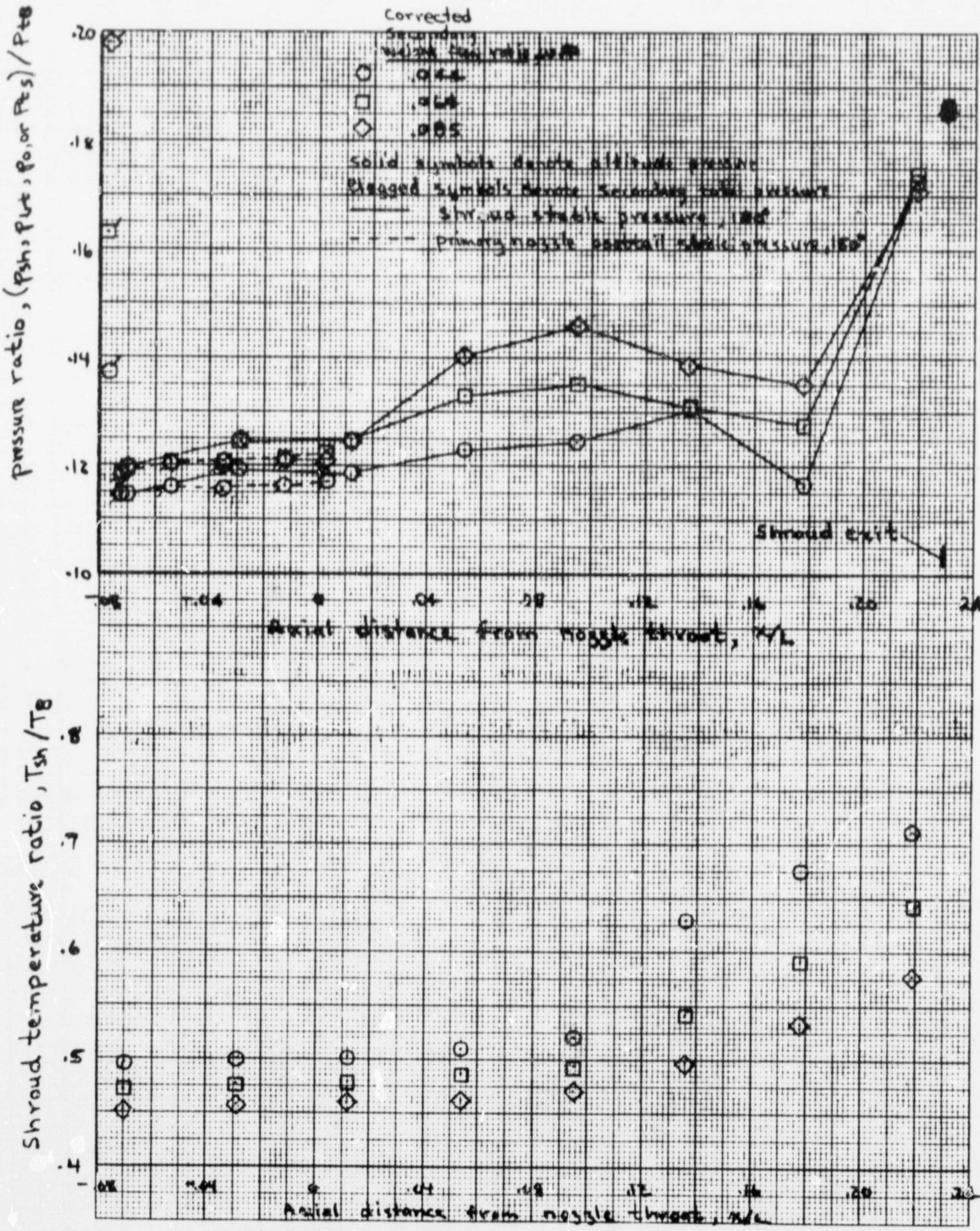

a.) Nozzle pressure ratio = 5.4.

Figure 13.- Typical pressure and temperature distributions on the shroud and primary nozzle boattail. Shroud, $x/L = 0.229$.

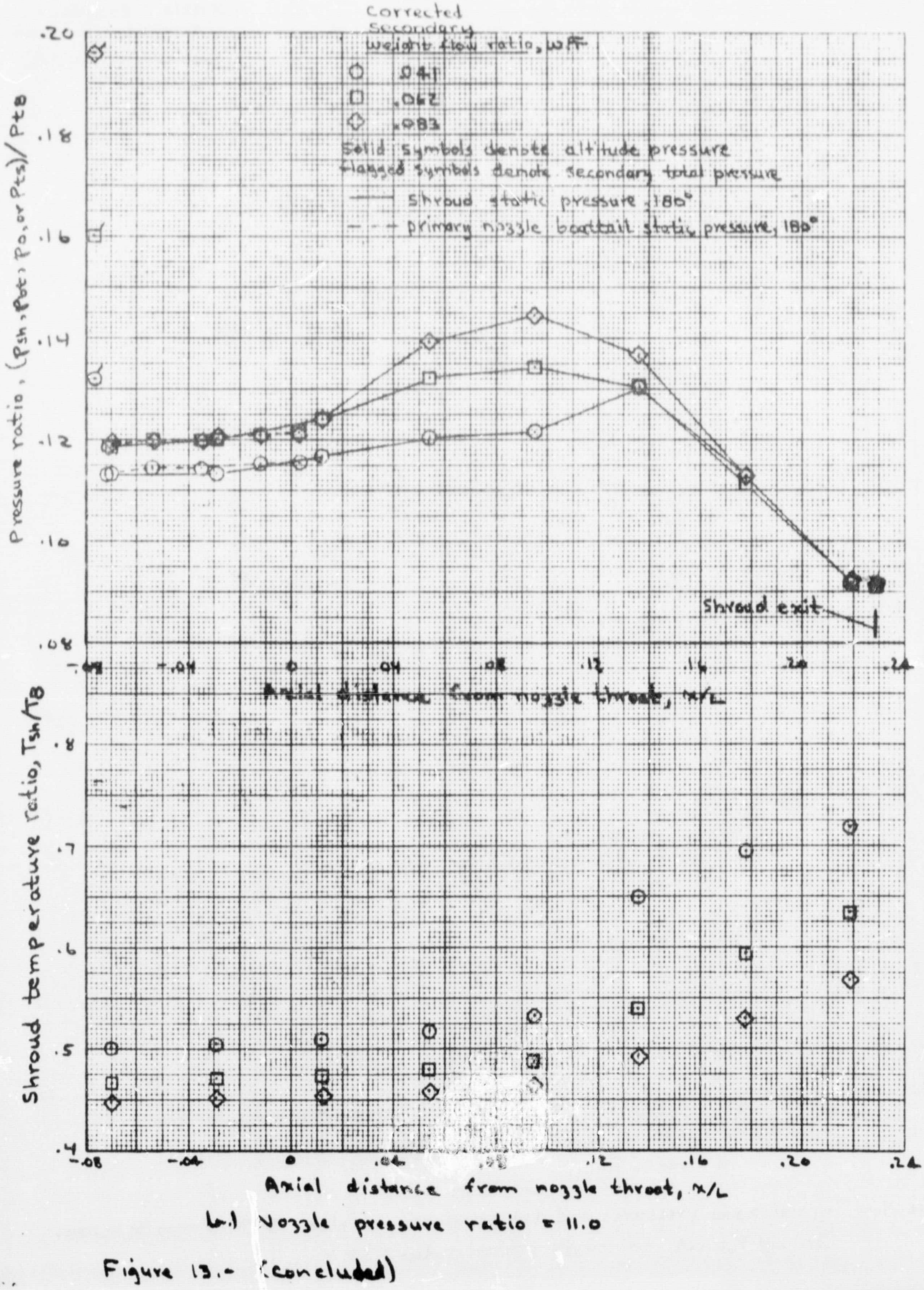

(b) Nozzle pressure ratio = 11.0

Figure 13.- (Concluded)

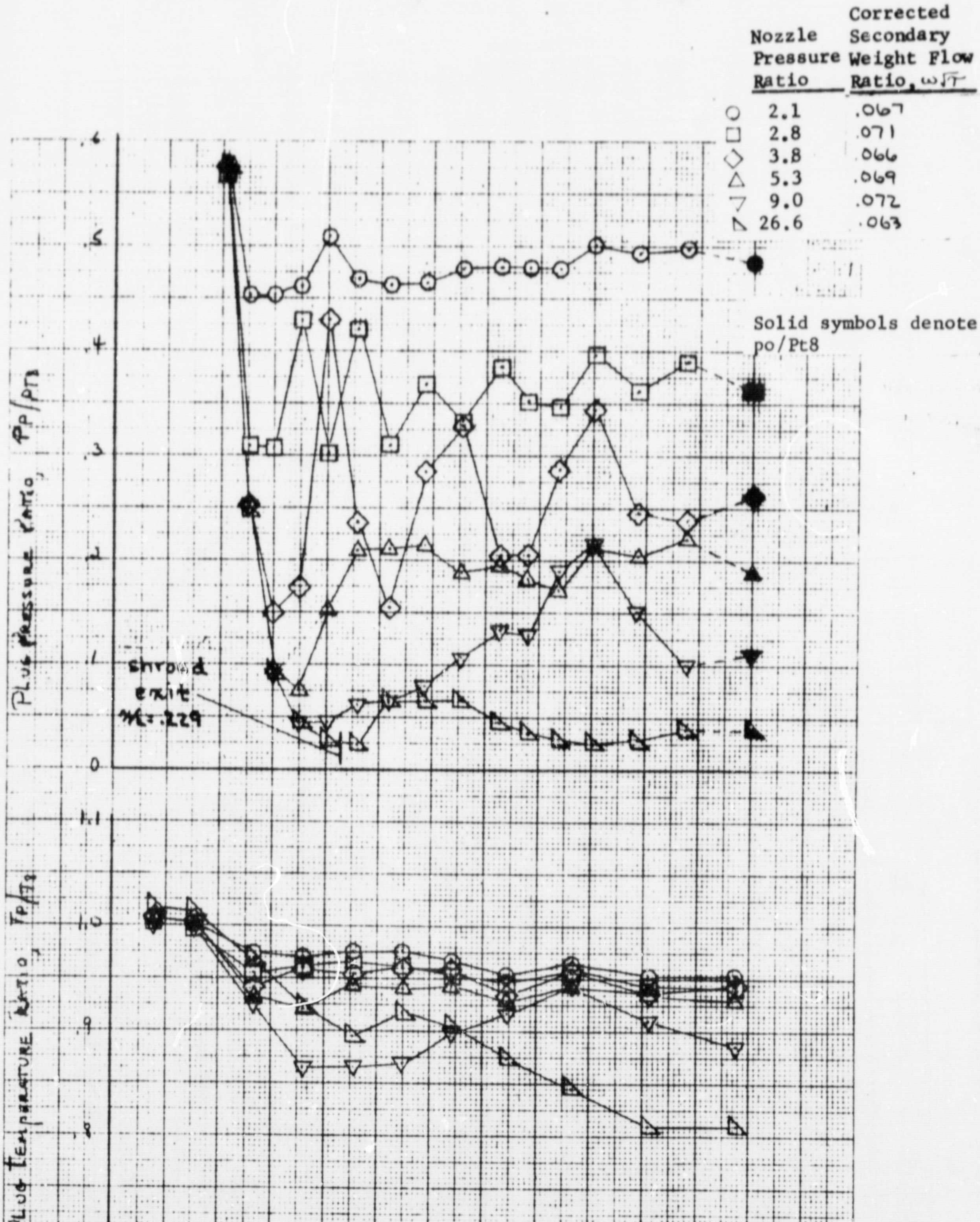

a.) 100% plug.

Figure 14.- Typical axial pressures and temperatures on plug. ϕ=90°, shroud x/L=-.080. (Shroud x/L=.229 for nozzle pressure ratios > 25)

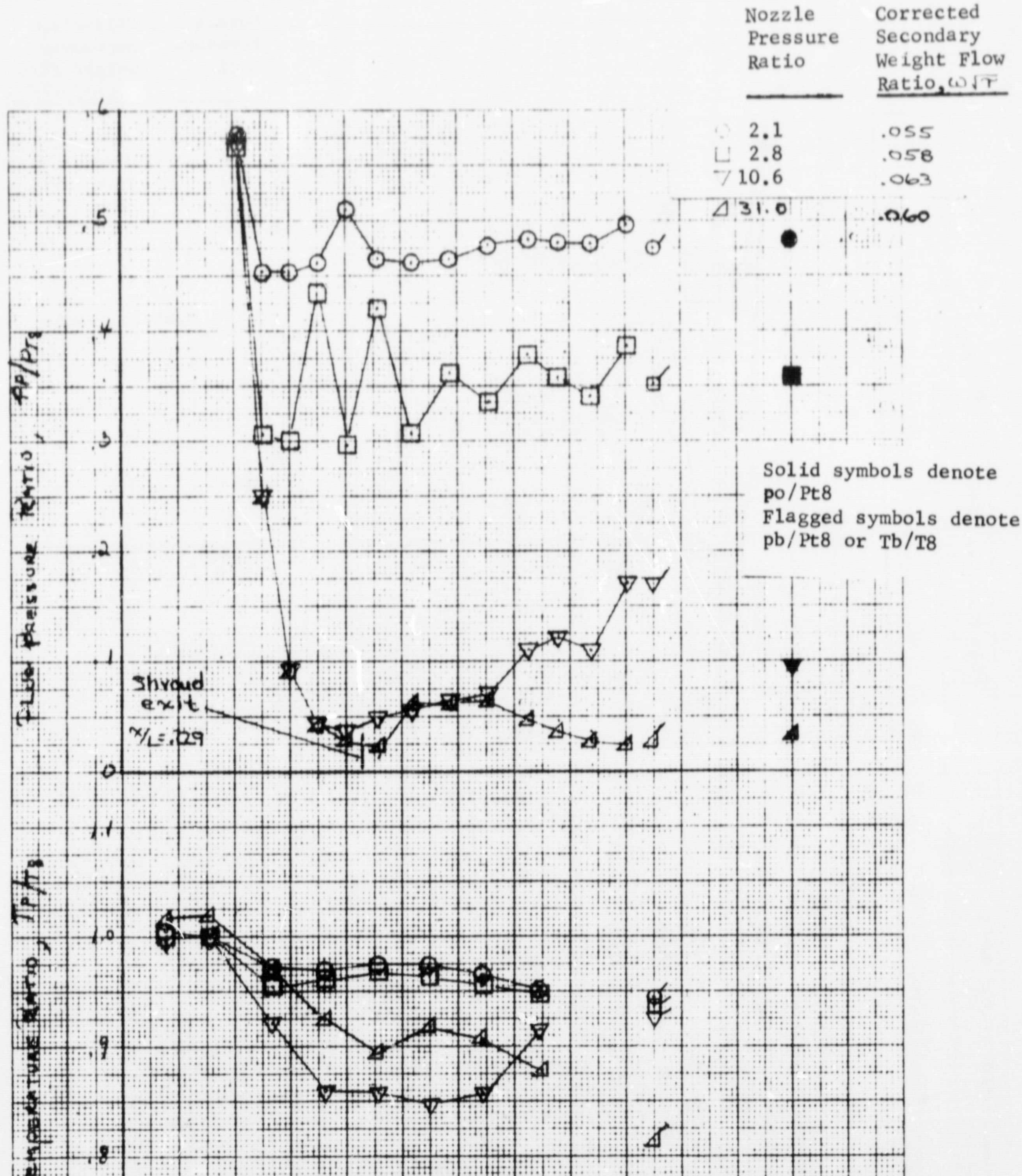

b) 75% Plug.

Figure 14 - (continued)

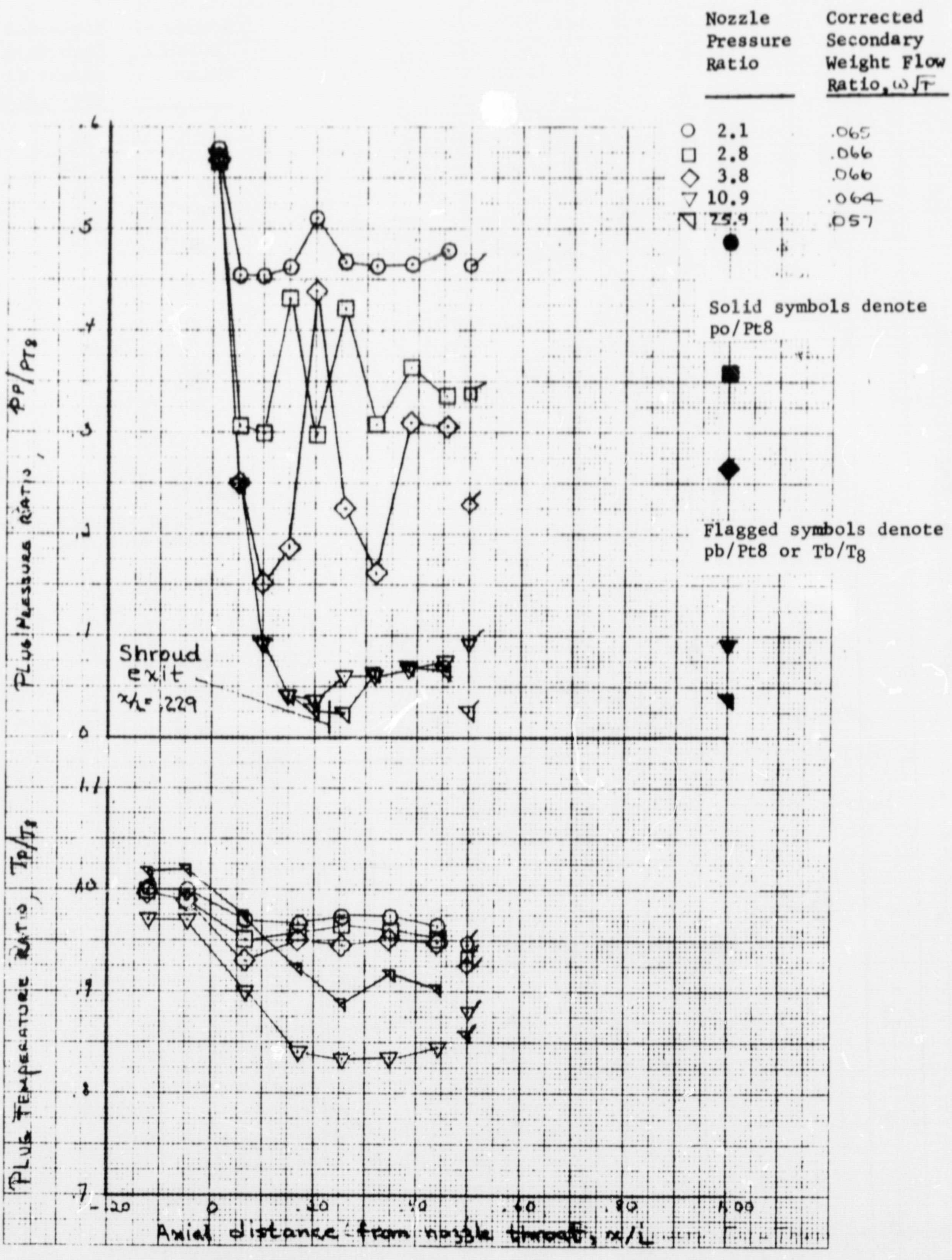

c.) 50% Plug.

Figure 14.- (concluded)

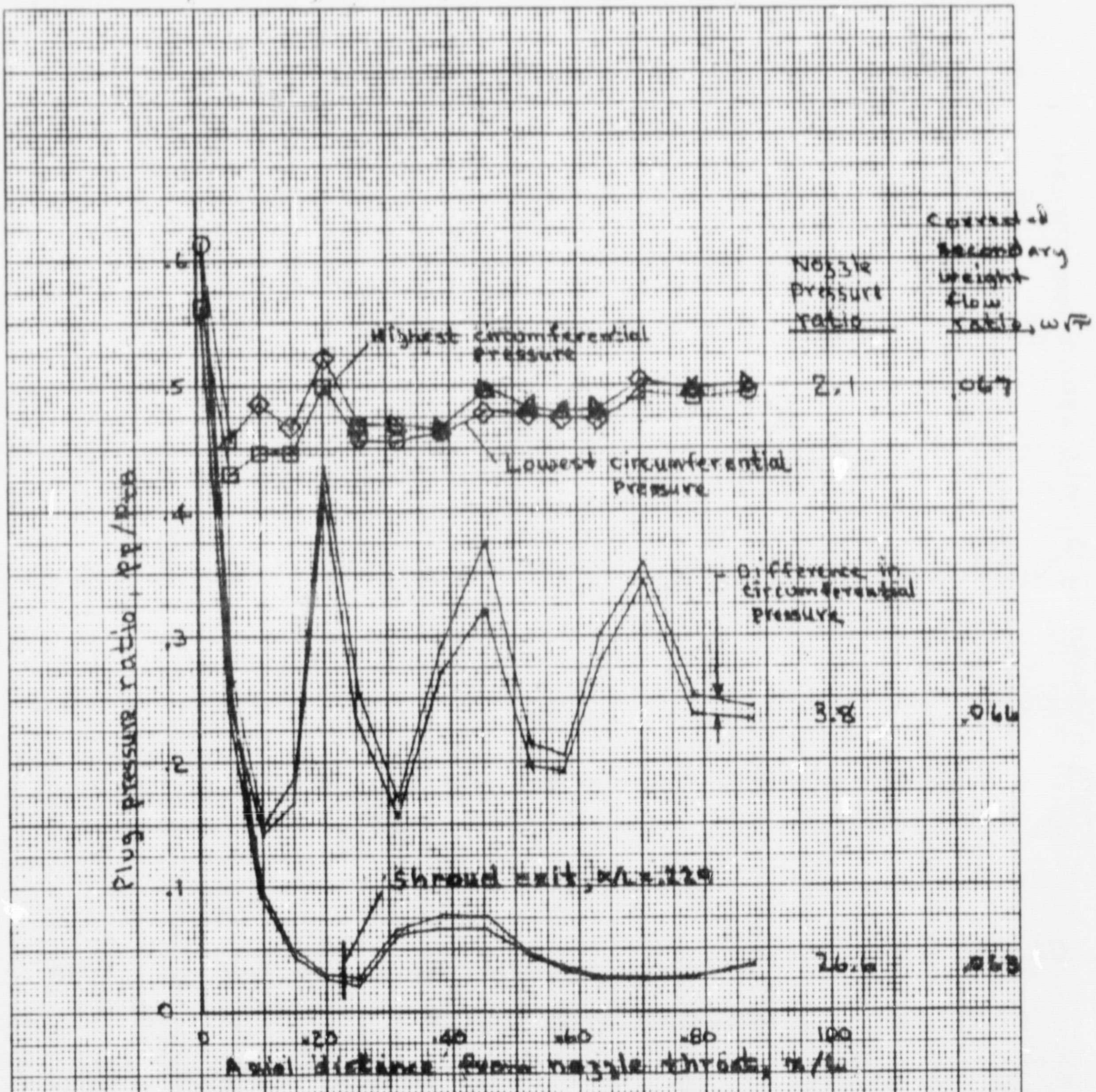

Figure 15. - Typical difference in circumferential pressure along plug. (x/L = .030 and .229 shrouds).

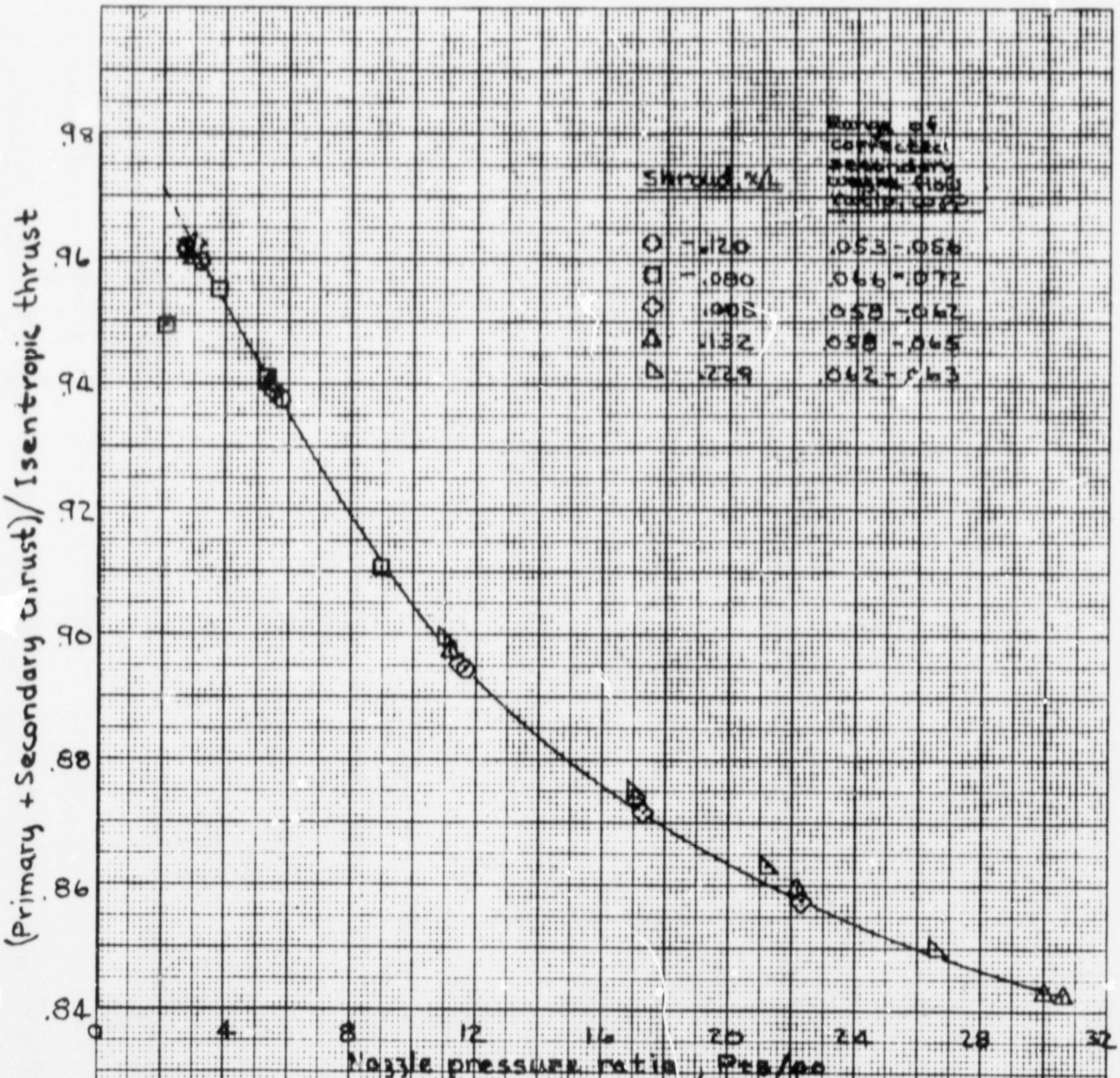

Figure 16. - Sum of calculated primary and secondary thrust. 100% plug.

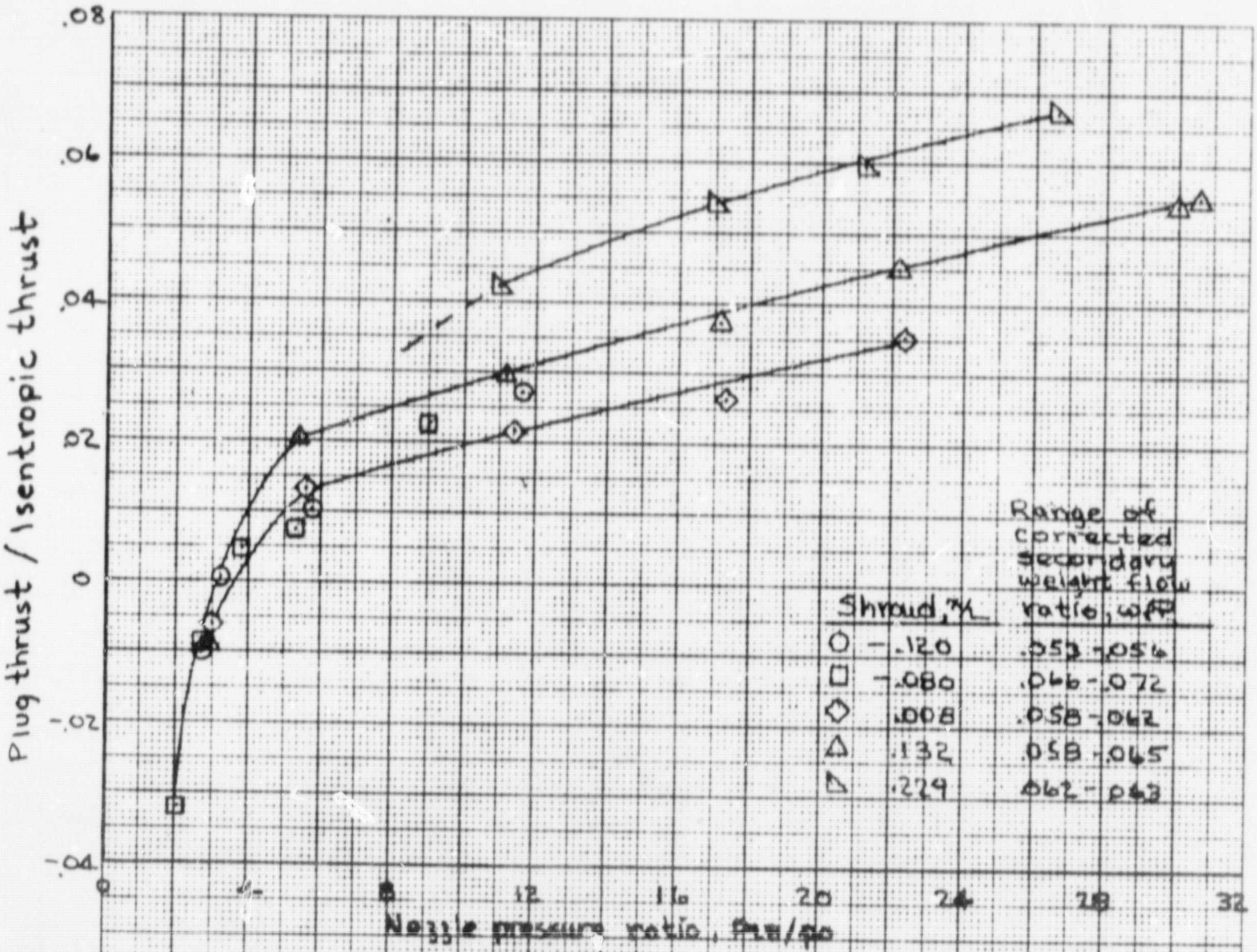

a.) 100% plug.

Figure 17.- Thrust contribution of plug (and base of truncated plugs).

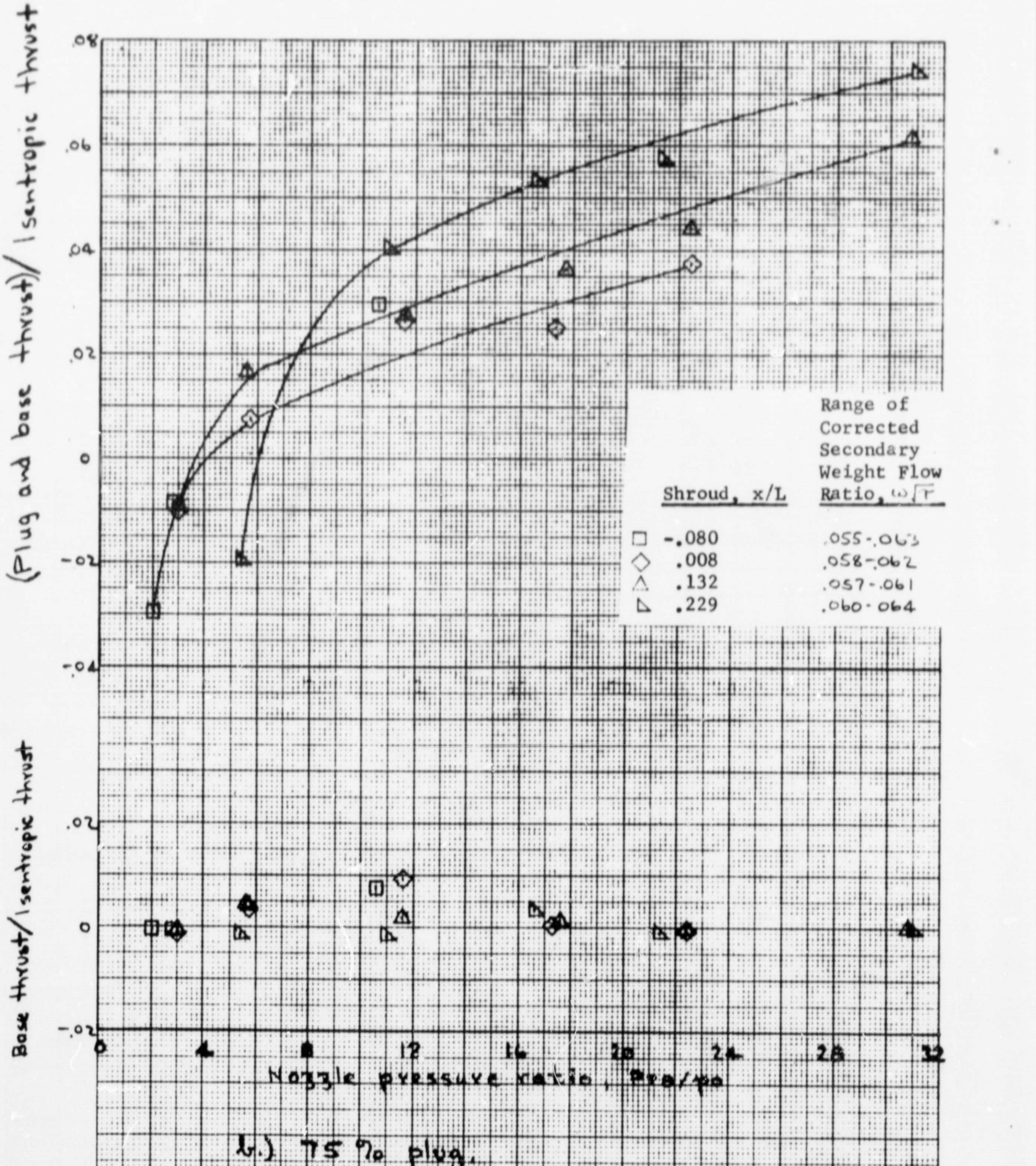

Figure 17.- (continued).

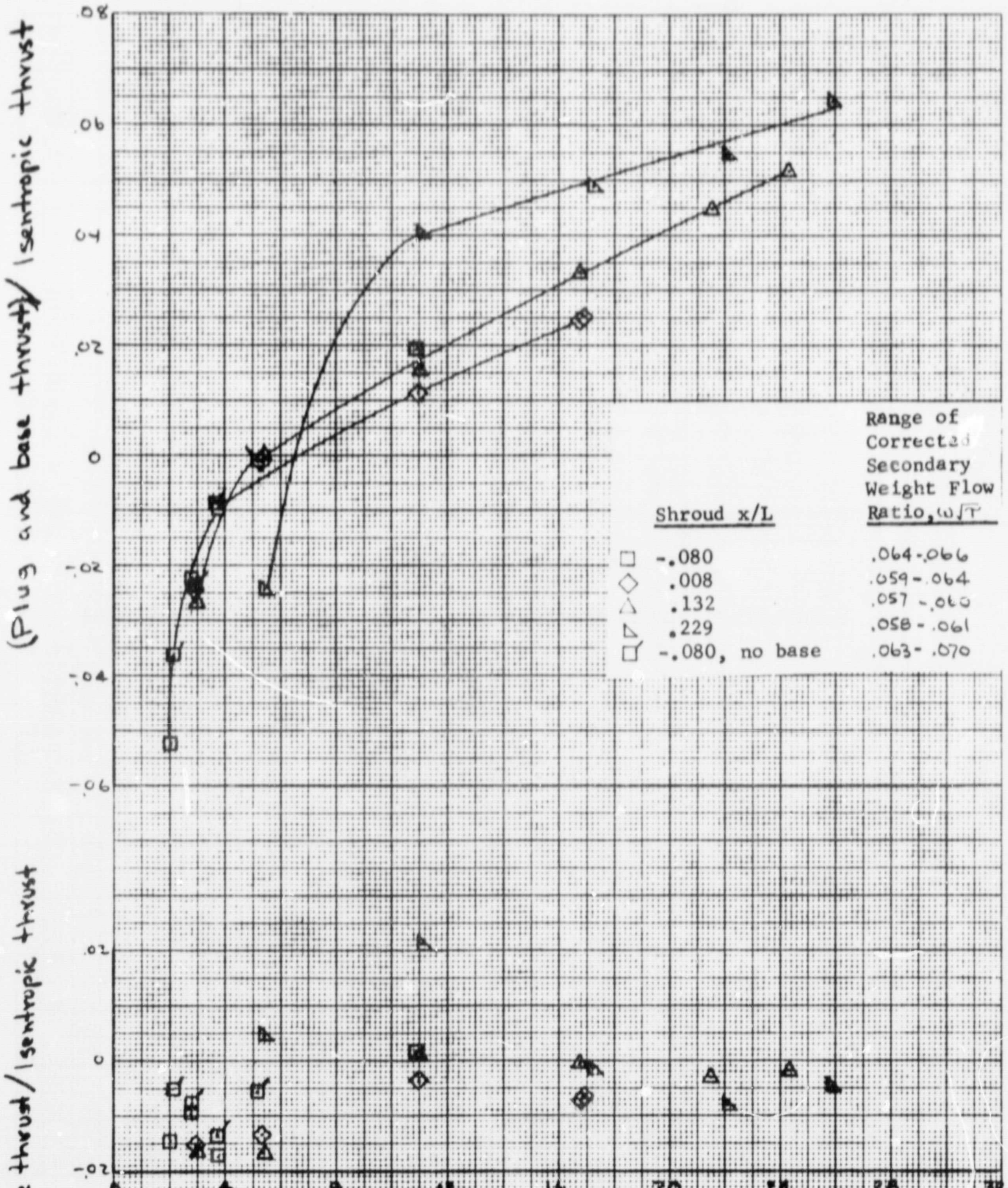

c.) 50% plug.

Figure 17.- (concluded).

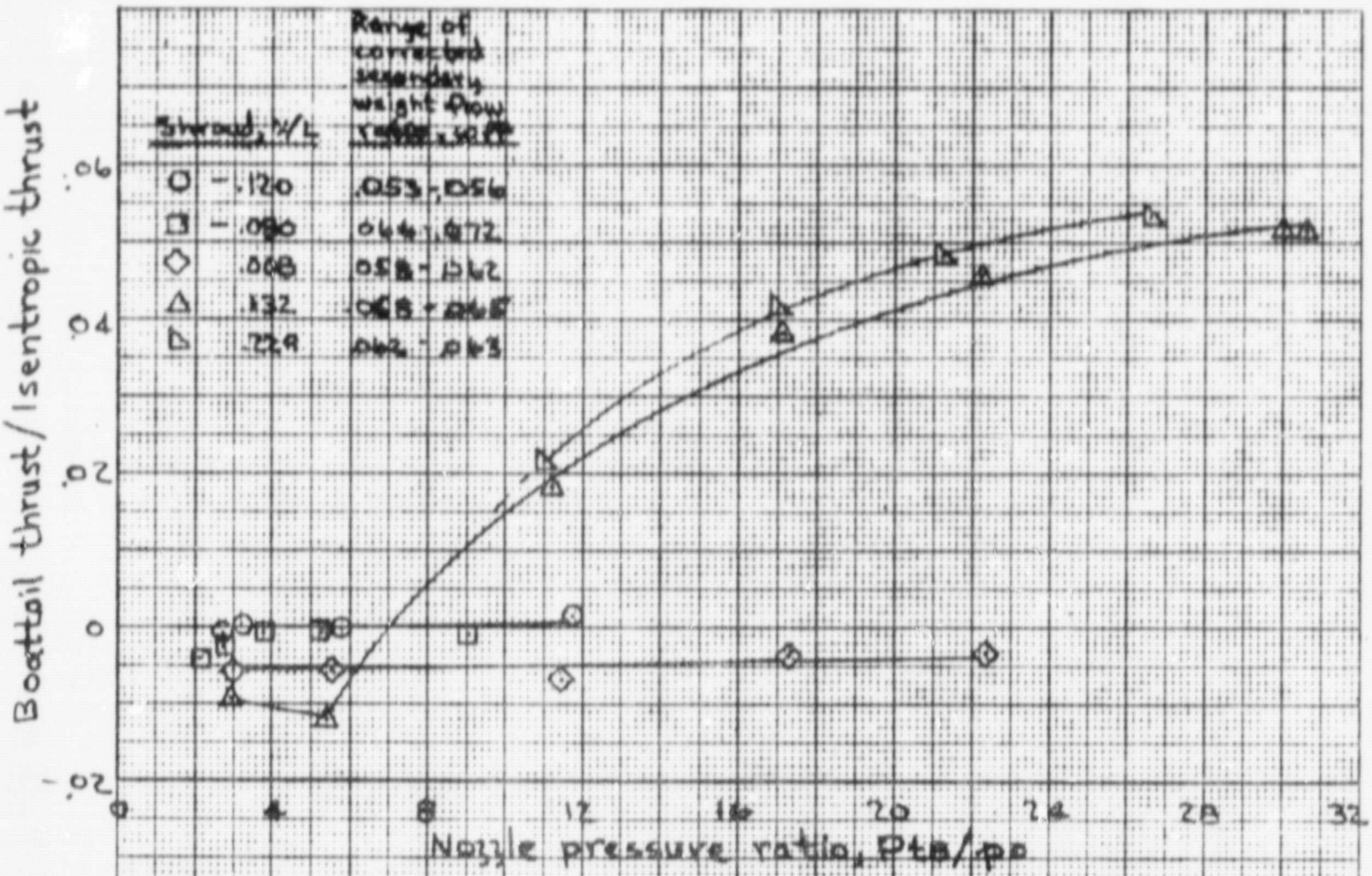

Figure 18.- Thrust contribution of primary nozzle boattail. 100% plug.

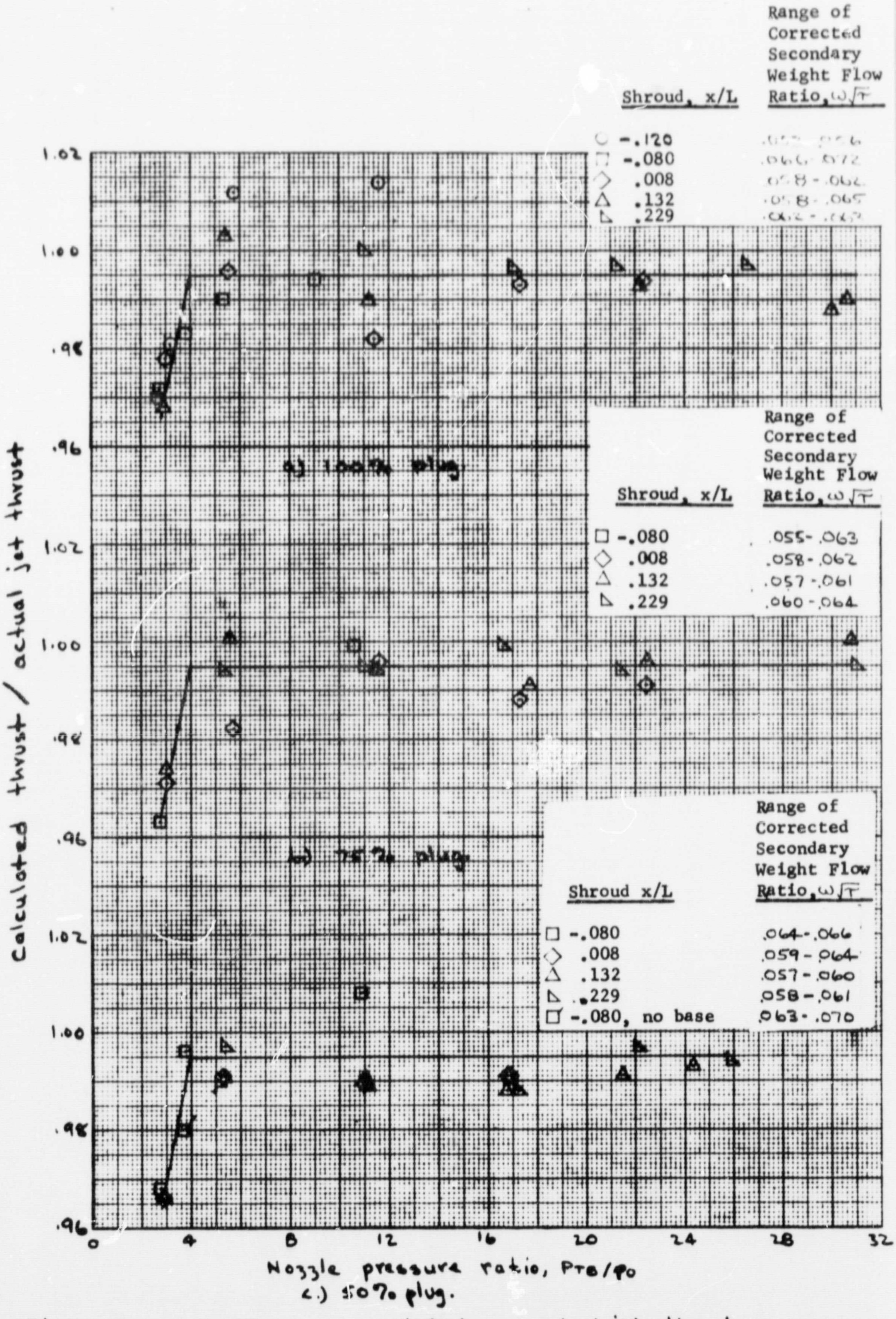

Figure 19.- Comparison of calculated and actual jet thrust.